This is the accepted manuscript made available via CHORUS. The article has been published as:

Photoinduced superconductivity in semiconductors

Garry Goldstein, Camille Aron, and Claudio Chamon

Phys. Rev. B **91**, 054517 — Published 24 February 2015

DOI: 10.1103/PhysRevB.91.054517

Photo-induced superconductivity in semiconductors

Garry Goldstein,[1] Camille Aron,[1,2] and Claudio Chamon[3]

[1]*Department of Physics, Rutgers University, Piscataway, New Jersey 08854, USA*
[2]*Department of Electrical Engineering, Princeton University, Princeton, New Jersey 08544, USA*
[3]*Department of Physics, Boston University, Boston, Massachusetts 02215, USA*

We show that optically pumped *semiconductors* can exhibit superconductivity. We illustrate this phenomenon in the case of a two-band semiconductor tunnel-coupled to broad-band reservoirs and driven by a continuous wave laser. More realistically, we also show that superconductivity can be induced in a two-band semiconductor interacting with a broad-spectrum light source. We furthermore discuss the case of a three-band model in which the middle band replaces the broad-band reservoirs as the source of dissipation. In all three cases, we derive the simple conditions on the band structure, electron-electron interaction, and hybridization to the reservoirs that enable superconductivity. We compute the finite superconducting pairing and argue that the mechanism can be induced through both attractive and repulsive interactions and is robust to high temperatures.

I. INTRODUCTION

Superconductivity is unarguably a fascinating phase of matter with tremendous applications. This low-temperature instability towards zero-resistivity corresponds to the emergence and the condensation of Cooper pairs of electrons. In most simple metallic systems, the pairing is achieved by phonon-mediated interactions[1] and the superconducting temperature does not exceed a few Kelvin. The last fifty years have seen some remarkable progress in the understanding of superconductivity. Cuprates[2] and iron pnictides[3,4] now offer critical temperatures on the order of a hundred Kelvin. They were dubbed "high-temperature superconductors" as such temperatures can be easily achieved with liquid nitrogen. All this allowed superconductivity to become a cornerstone to many modern technological developments[1]. The Josephson effect is routinely used in superconducting quantum interference devices (SQUIDs)[1], and its inherent non-linearity is widely used to build qubits[5,6]. The Meissner effect and the zero resistivity are used to realize powerful magnets[7]. However, the search for room-temperature superconductivity is still a very active field of research[8].

Pioneering examples of the use of AC microwave fields in condensed matter systems have been to enhance the critical temperature of regular superconductors by redistributing the quasiparticle density near the Fermi surface[1]. More recently, it was established that an AC electric field leads to a renormalization of the lattice hopping parameters[9–11]. It has been suggested that in interacting systems such as the Bose-Hubbard model it is thereby possible to induce a superfluid Mott insulator phase transition[12–14]. Reversing the signs of the hoppings in a lattice model could be used to realize frustrated classical spin systems[15]. In the case of electrons driven by a laser field, many interesting phenomena have been proposed[16,17]. These include dynamical band flipping and splitting[18], interaction strength renormalization, changes in the sign of the effective interaction strength leading to s-wave superconductivity with repulsive bare interactions and negative absolute temperatures for a laser-driven band model.

In this work, we envision a novel route to achieve superconductivity which consists of optically driving a two-band *semiconductor* to a suitable non-equilibrium steady state which supports *interband* pairing between electrons in the valence and conduction electrons. Importantly, we shall demonstrate the robustness of this mechanism with respect to temperature, up to room temperature, as long as it is smaller than the semiconducting gap.

We note that the possibility of inducing superconductivity in a two band model has been discussed in narrow, indirect gap semiconductors.[19–23] However the mechanism proposed here is significantly different in that it involves *interband* pairing for wide gap semiconductors, instead of *intraband* pairing for narrow gap semiconductors. Furthermore, in our mechanism the majority of the pairing occurs around a resonant surface $\mathcal{S}_{\omega_0}$ (see Section II) which is not directly related to the band edge. Among the chief consequences of the difference in pairing channel and its k-space location is the fact that in our mechanism the pairing amplitude does not need to be larger than the semiconducting gap in order to establish non-equilibrium steady-state superconductivity, therefore making pairing more easily attainable.

In Sect. II, we take a pedagogical route to demonstrate this effect by considering a model of a two-band semiconductor in tunneling contact with two reservoirs provided, say, by a metallic plate [see Fig. (1)]. We carefully show that it is possible to induce superconductivity in this system under favorable conditions involving the electronic dispersion, the electron-electron interaction, and the hybridizations to the reservoirs as well as the chemical potential. To support the validity of our analytical results in the steady-state, we perform an exact numerical integration of the time dynamics. We show in particular that the predicted non-trivial steady state is indeed reached dynamically.

In Sect. III, we argue that the previous case can be reduced to a simpler yet more realistic model of a two-band semiconductor – not in strong tunneling contact with any engineered external reservoirs – which is optically pumped by a broad-band light source. In many ways, it is the most relevant model discussed in this manuscript and the reader

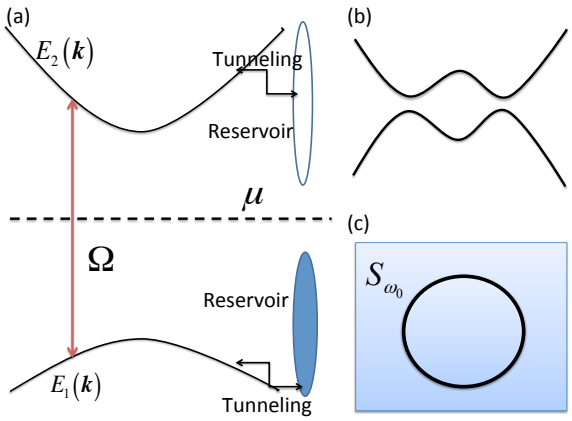

FIG. 1: Energy levels and laser. (a) A continuous wave laser drives transitions between the lower (1) and upper (2) bands. Both bands are coupled to reservoirs. The chemical potentials of the reservoirs μ is set in the gap. (b) In the rotating frame, the laser induces an avoided band crossing (with splitting $\sim |\Omega|$). (c) This creates an effective resonant surface $\mathcal{S}_{\omega_0}$ consisting of the set of momenta $\boldsymbol{k}_0$ for which the laser resonantly connects the two bands.

eager to learn about these results can directly jump to Sect. III which is written in a self-contained fashion.

In Sect. IV, we provide an alternative derivation of the previous results by means of a Keldysh formalism approach. In particular, this allows to justify properly an approximation used to self-consistently compute the superconducting pairing.

For the sake of completeness, we review in the Appendix the case of a three-band semiconductor in which the extra band plays the role of the reservoirs in Sect II.

II. LASER-DRIVEN DISSIPATIVE TWO-BAND SEMICONDUCTOR

Let us consider a semiconductor with two relevant electronic bands: the lower band ($\alpha = 1$) with dispersion $E_1(\boldsymbol{k})$ and the upper band ($\alpha = 2$) with dispersion $E_2(\boldsymbol{k})$ are separated by a gap $E_{\rm g}$. For the sake of simplicity, let us assume that the dispersion is symmetric so that $E_\alpha(\boldsymbol{k}) = E_\alpha(-\boldsymbol{k})$ for both bands $\alpha = 1, 2$; this will allow for s-wave superconductivity without any energy mismatches. The semiconductor is driven by a continuous coherent laser source with frequency ω_0. This induces transitions between the bands if there are momenta $\boldsymbol{k}_0$ such that $E_2(\boldsymbol{k}_0) = E_1(\boldsymbol{k}_0) + \omega_0$. In practice this condition is easily met and the corresponding momenta lie on a finite closed surface $\mathcal{S}_{\omega_0}$ of the Brillouin zone. In particular we assume that the level surfaces of $E_1(\boldsymbol{k}_0)$ and $E_2(\boldsymbol{k}_0)$ have good overlap (which would happen for say parabolic bands). The laser acts as a source of energy and we provide a heat sink by coupling each band to an independent reservoir which can exchange particles and energy. Both reservoirs are kept in equilibrium at temperature T and chemical potential μ. In principle, one can also consider a single reservoir provided that its density of state is broad enough to overlap with the upper and lower bands. We set the chemical potential in the gap, exactly halfway between the two bands, $\mu = [E_2(\boldsymbol{k}_0) + E_1(\boldsymbol{k}_0)]/2$. This ensures that all quasiparticles have zero energy. In the rotating frame, this will correspond to a zero-energy condition for the electrons at $\boldsymbol{k}_0 \in \mathcal{S}_{\omega_0}$. Below, we measure energies relative to μ, *i.e.* we set $\mu = 0$. We shall see later that the ability for the electronic bands to acquire non-trivial populations is crucial to the occurrence of superconductivity. In the case at hand, this is favored if the two reservoirs have different density of states or different coupling strength to the bands. In the Appendix, we shall see that a third band, or alternatively as in Sect. III, other $\boldsymbol{k}$ modes in the same band can also play this role.

In order to establish that superconductivity can be realized in such a driven-dissipative system, we first solve for its non-equilibrium steady-state dynamics by means of a Master equation approach. Within a self-consistent mean-field approach, we then obtain the criteria for superconducting pairing and estimate the size of the superconducting gap. Finally, we discuss the robustness of our results, in particular against finite temperature.

A. Mean-field Hamiltonian and Master Equation

We decompose the total model Hamiltonian into a laser-driven semiconductor part (the system), a reservoir part (the bath), and a system-reservoir coupling part:

$$H = H_{\rm sys} + H_{\rm bath} + H_{\rm sys-bath} \tag{1}$$

where

$$\begin{aligned} H_{\rm sys} =& \sum_{\boldsymbol{k},\alpha} E_\alpha(\boldsymbol{k})\, c_{\boldsymbol{k}}^{\alpha\dagger}\, c_{\boldsymbol{k}}^{\alpha} + \Omega(t) \sum_{\boldsymbol{k},\alpha,\beta} c_{\boldsymbol{k}}^{\alpha\dagger}\, \sigma^x_{\alpha\beta}\, c_{\boldsymbol{k}}^{\beta} \\ &+ \frac{\mathrm{i}}{2}\Delta \sum_{\boldsymbol{k},\alpha,\beta} c_{\boldsymbol{k}}^{\alpha\dagger}\, \sigma^y_{\alpha\beta}\, c_{-\boldsymbol{k}}^{\beta\,\dagger} - \frac{\mathrm{i}}{2}\Delta^* \sum_{\boldsymbol{k},\alpha,\beta} c_{\boldsymbol{k}}^{\alpha}\, \sigma^y_{\alpha\beta}\, c_{-\boldsymbol{k}}^{\beta}, \end{aligned} \tag{2}$$

$$H_{\rm bath} = \sum_{\boldsymbol{k},n,\alpha} \omega_n^\alpha(\boldsymbol{k})\, a_{\boldsymbol{k},n}^{\alpha\,\dagger}\, a_{\boldsymbol{k},n}^{\alpha}\ , \tag{3}$$

and

$$H_{\rm sys-bath} = \sum_{\boldsymbol{k},n,\alpha} t_\alpha(\boldsymbol{k})\ \left[c_{\boldsymbol{k}}^{\alpha\dagger} a_{\boldsymbol{k},n}^{\alpha} + a_{\boldsymbol{k},n}^{\alpha\,\dagger}\, c_{\boldsymbol{k}}^{\alpha}\right]\ . \tag{4}$$

$c_{\boldsymbol{k}}^{\alpha}$ and $c_{\boldsymbol{k}}^{\alpha\dagger}$ are the creation and annihilation operators of electrons with a quasi-momentum $\boldsymbol{k}$ in the α band, $\alpha = 1, 2$. $\Omega\,(t) = \Omega\cos(\omega_0 t)$ is the laser drive, and $\sigma^{x,y,z}$ are the usual Pauli matrices acting on the band indices. The last two terms in $H_{\rm sys}$ originate from a microscopic electron-electron interaction which we treat at a mean-field level (see also Sect. II b). Δ is the complex order parameter which quantifies the superconducting pairing between the bands and that will be determined self-consistently. The $a_{\boldsymbol{k},n}^{\alpha}$'s represent the degrees of freedom of the non-interacting reservoirs with energy ω_n^α. Here n is a mode label. We shall assume that the reservoirs have continuous density of states given by $\nu_\alpha(\omega)$ and that they are weakly coupled to the system, *i.e.* $\left|t_\alpha^2\right| \nu_\alpha \ll E_2 - E_1$[24]. In this case, the dynamics of the reduced density matrix of the system, $\rho_{\rm sys}$, can be described by a Master equation reading[25]

$$\frac{\mathrm{d}}{\mathrm{d}t}\,\rho_{\rm sys} = -\,\mathrm{i}\,[H_{\rm sys}, \rho_{\rm sys}] + \sum_{\boldsymbol{k},\alpha} \Gamma_\alpha\,(\boldsymbol{k})\,\left[n_F\,(E_\alpha\,(\boldsymbol{k}))\,\mathcal{D}[c_{\boldsymbol{k}}^{\alpha\dagger}]\rho_{\rm sys} + (1 - n_F\,(E_\alpha\,(\boldsymbol{k})))\,\mathcal{D}[c_{\boldsymbol{k}}^{\alpha}]\rho_{\rm sys}\right]\ , \tag{5}$$

where $n_{\rm F}(\epsilon) \equiv [1 + \exp(\epsilon/T)]^{-1}$ is the Fermi-Dirac distribution function, and the rates $\Gamma_\alpha(\boldsymbol{k}) \equiv \pi\,|t_\alpha(\boldsymbol{k})|^2\,\nu_\alpha\big(E_\alpha(\boldsymbol{k})\big)$ are given by Fermi's golden rule. We note that for some decaying mechanisms such as phonons not considered here, the rates Γ_1 and Γ_2 may be temperature dependent. The Lindblad-type dissipators are defined as $\mathcal{D}[X]\rho \equiv \big(X\rho X^\dagger - X^\dagger X\rho + \text{h.c.}\big)/2$. We neglected the Lamb-shift corrections (real part of hybridization self-energy). We may now write the equations of motion for the populations, coherences and anomalous correlators $n_{\boldsymbol{k}}^{\alpha\beta} \equiv \langle c_{\boldsymbol{k}}^{\alpha\dagger}\, c_{\boldsymbol{k}}^{\beta}\rangle$ and $s_{\boldsymbol{k}}^{\alpha\beta} \equiv \langle c_{\boldsymbol{k}}^{\alpha\dagger}\, c_{-\boldsymbol{k}}^{\beta\,\dagger}\rangle$ with $\alpha, \beta = 1, 2$:

$$\frac{\mathrm{d}}{\mathrm{d}t} n_{\boldsymbol{k}}^{11} \;=\; -\mathrm{i}\Omega(t)\left(n_{\boldsymbol{k}}^{12} - n_{\boldsymbol{k}}^{21}\right) + \mathrm{i}\Delta\, s_{\boldsymbol{k}}^{21} - \mathrm{i}\Delta^*\, s_{\boldsymbol{k}}^{21\,*} - 2\Gamma_1(\boldsymbol{k})\left[n_{\boldsymbol{k}}^{11} - n_{\rm F}\big(E_1(\boldsymbol{k})\big)\right], \tag{6a}$$

$$\frac{\mathrm{d}}{\mathrm{d}t} n_{\boldsymbol{k}}^{22} \;=\; -\mathrm{i}\Omega(t)\left(n_{\boldsymbol{k}}^{21} - n_{\boldsymbol{k}}^{12}\right) + \mathrm{i}\Delta\, s_{\boldsymbol{k}}^{21} - \mathrm{i}\Delta^*\, s_{\boldsymbol{k}}^{21\,*} - 2\Gamma_2(\boldsymbol{k})\left[n_{\boldsymbol{k}}^{22} - n_{\rm F}\big(E_2(\boldsymbol{k})\big)\right], \tag{6b}$$

$$\frac{\mathrm{d}}{\mathrm{d}t} n_{\boldsymbol{k}}^{21} \;=\; \mathrm{i}[E_2(\boldsymbol{k}) - E_1(\boldsymbol{k})]\, n_{\boldsymbol{k}}^{21} - \mathrm{i}\Omega(t)\left(n_{\boldsymbol{k}}^{22} - n_{\boldsymbol{k}}^{11}\right) - [\Gamma_2(\boldsymbol{k}) + \Gamma_1(\boldsymbol{k})]\, n_{\boldsymbol{k}}^{21}, \tag{6c}$$

$$\frac{\mathrm{d}}{\mathrm{d}t} s_{\boldsymbol{k}}^{21} \;=\; \mathrm{i}[E_2(\boldsymbol{k}) + E_1(\boldsymbol{k})]\, s_{\boldsymbol{k}}^{21} + \mathrm{i}\Delta^*\left(n_{\boldsymbol{k}}^{11} + n_{\boldsymbol{k}}^{22} - 1\right) - [\Gamma_2(\boldsymbol{k}) + \Gamma_1(\boldsymbol{k})]\, s_{\boldsymbol{k}}^{21}\ , \tag{6d}$$

in which we made use of the identity $\mathrm{tr}\big(O\,\mathcal{D}[X]\rho\big) = \mathrm{tr}\big([X^\dagger, O]X\rho\big) + \mathrm{tr}\big(X^\dagger[O, X]\rho\big) = \langle[X^\dagger, O]X\rangle_\rho + \langle X^\dagger[O, X]\rangle_\rho$ repeatedly. We then perform a rotating wave approximation (RWA) to eliminate the explicit time dependence of these equations. This consists in rotating all the operators of the theory with the unitary

$$U \equiv U_c \otimes U_a\ , \tag{7}$$

where

$$U_c \equiv \exp\left[\frac{\mathrm{i}}{2}\omega_0 t \sum_{\boldsymbol{k}} \left(c^{1\dagger}_{\boldsymbol{k}} c^{1}_{\boldsymbol{k}} - c^{2\dagger}_{\boldsymbol{k}} c^{2}_{\boldsymbol{k}}\right)\right] \text{ and } U_a \equiv \exp\left[\frac{\mathrm{i}}{2}\omega_0 t \sum_{\boldsymbol{k},n} \left(a^{1\dagger}_{\boldsymbol{k},n} a^{1}_{\boldsymbol{k},n} - a^{2\dagger}_{\boldsymbol{k},n} a^{2}_{\boldsymbol{k},n}\right)\right] . \tag{8}$$

In particular, $c^1_{\boldsymbol{k}} \mapsto \widetilde{c}^1_{\boldsymbol{k}} = c^1_{\boldsymbol{k}}\,\mathrm{e}^{-\mathrm{i}\omega_0 t/2}$, $c^2_{\boldsymbol{k}} \mapsto \widetilde{c}^2_{\boldsymbol{k}} = c^2_{\boldsymbol{k}}\,\mathrm{e}^{\mathrm{i}\omega_0 t/2}$, and $H \mapsto \widetilde{H} = U\left[H - \mathrm{i}\partial_t\right]U^\dagger$ so that the energies are shifted to $\widetilde{E}_1(\boldsymbol{k}) = E_1(\boldsymbol{k}) + \omega_0/2$ and $\widetilde{E}_2(\boldsymbol{k}) = E_2(\boldsymbol{k}) - \omega_0/2$. Note that in the rotating frame, $\widetilde{n}^{11}_{\boldsymbol{k}} = n^{11}_{\boldsymbol{k}}$, $\widetilde{n}^{22}_{\boldsymbol{k}} = n^{22}_{\boldsymbol{k}}$, and $\widetilde{s}^{12}_{\boldsymbol{k}} = s^{12}_{\boldsymbol{k}}$ are invariant, but $\widetilde{n}^{12}_{\boldsymbol{k}} = n^{12}_{\boldsymbol{k}}\,\mathrm{e}^{-\mathrm{i}\omega_0 t}$ and $\widetilde{n}^{21}_{\boldsymbol{k}} = n^{21}_{\boldsymbol{k}}\,\mathrm{e}^{\mathrm{i}\omega_0 t}$. We drop all terms rotating at $2\omega_0$ since they are not resonant with any transition. We also drop the $\boldsymbol{k}$-dependence of the decay rates $\Gamma_{1,2}(\boldsymbol{k}) \to \Gamma_{1,2}$, which is justified by assuming their weak momentum dependence in the small window of momenta around the surface of resonant condition $\mathcal{S}_{\omega_0}$. Altogether, we obtain

$$\frac{\mathrm{d}}{\mathrm{d}t}\widetilde{n}^{11}_{\boldsymbol{k}} = -\frac{\mathrm{i}}{2}\Omega\left(\widetilde{n}^{12}_{\boldsymbol{k}} - \widetilde{n}^{21}_{\boldsymbol{k}}\right) + \mathrm{i}\Delta\,\widetilde{s}^{21}_{\boldsymbol{k}} - \mathrm{i}\Delta^*\,\widetilde{s}^{21\,*}_{\boldsymbol{k}} - 2\Gamma_1\left[\widetilde{n}^{11}_{\boldsymbol{k}} - n_{\mathrm{F}}\big(E_1(\boldsymbol{k})\big)\right] , \tag{9a}$$

$$\frac{\mathrm{d}}{\mathrm{d}t}\widetilde{n}^{22}_{\boldsymbol{k}} = -\frac{\mathrm{i}}{2}\Omega\left(\widetilde{n}^{21}_{\boldsymbol{k}} - \widetilde{n}^{12}_{\boldsymbol{k}}\right) + \mathrm{i}\Delta\,\widetilde{s}^{21}_{\boldsymbol{k}} - \mathrm{i}\Delta^*\,\widetilde{s}^{21\,*}_{\boldsymbol{k}} - 2\Gamma_2\left[\widetilde{n}^{22}_{\boldsymbol{k}} - n_{\mathrm{F}}\big(E_2(\boldsymbol{k})\big)\right] , \tag{9b}$$

$$\frac{\mathrm{d}}{\mathrm{d}t}\widetilde{n}^{21}_{\boldsymbol{k}} = (\mathrm{i}\varepsilon_{\boldsymbol{k}} - \Gamma)\,\widetilde{n}^{21}_{\boldsymbol{k}} - \frac{\mathrm{i}}{2}\Omega\left(\widetilde{n}^{22}_{\boldsymbol{k}} - \widetilde{n}^{11}_{\boldsymbol{k}}\right) , \tag{9c}$$

$$\frac{\mathrm{d}}{\mathrm{d}t}\widetilde{s}^{21}_{\boldsymbol{k}} = (\mathrm{i}E_{\boldsymbol{k}} - \Gamma)\,\widetilde{s}^{21}_{\boldsymbol{k}} + \mathrm{i}\Delta^*\left(\widetilde{n}^{11}_{\boldsymbol{k}} + \widetilde{n}^{22}_{\boldsymbol{k}} - 1\right) , \tag{9d}$$

where we defined $\Gamma \equiv \Gamma_1 + \Gamma_2$, $\varepsilon_{\boldsymbol{k}} \equiv \widetilde{E}_2(\boldsymbol{k}) - \widetilde{E}_1(\boldsymbol{k})$, and $E_{\boldsymbol{k}} \equiv \widetilde{E}_2(\boldsymbol{k}) + \widetilde{E}_1(\boldsymbol{k})$. Where we have used the symmetry between $\boldsymbol{k}$ and $-\boldsymbol{k}$ stemming from $E_\alpha(\boldsymbol{k}) = E_\alpha(-\boldsymbol{k})$. This reduces all computations to just one wavevector $\boldsymbol{k}$.

The steady-state values of populations, coherences and anomalous correlators can now be solved by setting the left-hand side of Eqs. (9) to zero. We find that

$$\widetilde{s}^{21}_{\boldsymbol{k}} = -\frac{\Delta^*}{E_{\boldsymbol{k}} + \mathrm{i}\Gamma}\,\left(\widetilde{n}^{11}_{\boldsymbol{k}} + \widetilde{n}^{22}_{\boldsymbol{k}} - 1\right) , \tag{10}$$

where $\widetilde{n}^{11}_{\boldsymbol{k}} + \widetilde{n}^{22}_{\boldsymbol{k}} - 1$ measures the fraction of the total population that can be borrowed from, or shifted to, the "storage" constituted by the reservoirs or by the other $\boldsymbol{k}$ modes away from resonance. It is given by

$$\widetilde{n}^{11}_{\boldsymbol{k}} + \widetilde{n}^{22}_{\boldsymbol{k}} - 1 \approx \frac{\gamma_1 - \gamma_2}{\Xi}\frac{\Omega^2}{\epsilon^2_{\boldsymbol{k}} + \Gamma^2}\left[n_F\left(E_1(\boldsymbol{k})\right) - n_F\left(E_2\left(\boldsymbol{k}\right)\right)\right] , \tag{11}$$

where we defined $\gamma_{1,2} \equiv \Gamma_{1,2}/\Gamma$,

$$\Xi \equiv 4\gamma_1\gamma_2 + \frac{4|\Delta|^2}{{E_{\boldsymbol{k}}}^2 + \Gamma^2} + \frac{\Omega^2}{\epsilon^2_{\boldsymbol{k}} + \Gamma^2}\left[1 + \frac{4|\Delta|^2}{{E_{\boldsymbol{k}}}^2 + \Gamma^2}\right] , \tag{12}$$

and we neglected a term proportional to $n_{\mathrm{F}}\left(E_1(\boldsymbol{k})\right) + n_{\mathrm{F}}\left(E_2(\boldsymbol{k})\right) - 1$ since this factor vanishes at zero temperature and is exponentially suppressed for temperatures smaller than the semiconducting gap E_{g}. We note that both a large $\gamma_1\gamma_2$ and a large $|\Delta|$ lead to a decrease in $\widetilde{n}^{11}_{\boldsymbol{k}} + \widetilde{n}^{22}_{\boldsymbol{k}} - 1$.

Anticipating what follows, we shall see that only a non-vanishing value of $\widetilde{n}^{11}_{\boldsymbol{k}} + \widetilde{n}^{22}_{\boldsymbol{k}} - 1$, *i.e.* a finite population deviation from the equilibrium situation, will amount to superconductivity. It is quite transparent from Eq. (11) that in order to obtain such non-trivial band populations, one must drive the system ($\Omega \neq 0$) and the decay rates Γ_1 and Γ_2 must be different ($\gamma_1 \neq \gamma_2$).

When the drive Ω is large compared to Γ, the ratio $\Omega^2/(\epsilon^2_{\boldsymbol{k}} + \Gamma^2)$ is very large near the resonance ($\epsilon_{\boldsymbol{k}} = 0$). In this case, and when the temperature is much smaller than the semiconducting gap, the non-equilibrium population deviation simplifies to

$$\widetilde{n}^{11}_{\boldsymbol{k}} + \widetilde{n}^{22}_{\boldsymbol{k}} - 1 \approx \frac{E^2_{\boldsymbol{k}} + \Gamma^2}{E^2_{\boldsymbol{k}} + \Gamma^2 + 4|\Delta|^2}\,(\gamma_1 - \gamma_2) , \tag{13}$$

which holds in a range of width Ω near the resonance. We note that this approximation is also valid for moderate Ω when $\gamma_1\gamma_2 \cong 0$ and Δ is small. Hence, Ω plays the role of a cut-off, and for energies $|\epsilon_{\boldsymbol{k}}| < \Omega$ we can use the approximate expression in the equation above. Notice that one can achieve finite non-equilibrium population deviations in this range of $\epsilon_{\boldsymbol{k}}$, on the order of $\gamma_1 - \gamma_2$. Moreover, notice that the sign of this deviation depends on which of the decay rates Γ_1 or Γ_2 is larger, see also Fig. (2).

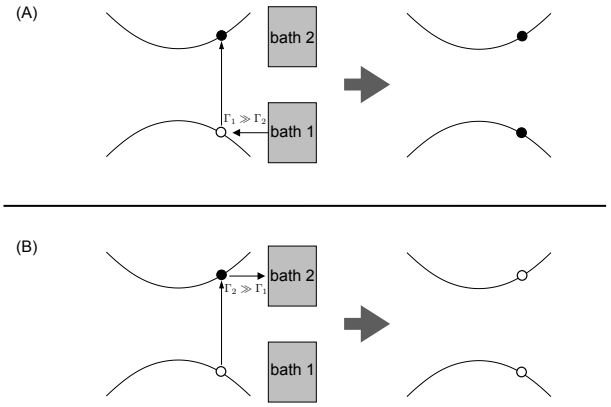

FIG. 2: Non-equilibrium population deviation due to driving and dissipation. The laser causes an electron in the valance band to transition into the conduction band. The figure illustrates particular examples when the two rates $\Gamma_{1,2}$ differ substantially. In (A), the rate $\Gamma_1 \gg \Gamma_2$, so the reservoirs fill the hole in the valance band much faster than the electron in the conduction band can relax back; the state is blocked, and one has $n_{\boldsymbol{k}}^{11} + n_{\boldsymbol{k}}^{22} - 1 \sim +1$. In (B), the rate $\Gamma_2 \gg \Gamma_1$, so the reservoirs remove the electron in the conduction band much faster than it can relax back; one is left with two holes, and one has $n_{\boldsymbol{k}}^{11} + n_{\boldsymbol{k}}^{22} - 1 \sim -1$ in this example.

In the opposite case in which the decay rate Γ is much larger than the drive Ω, the non-equilibrium population deviation is (for bath temperatures much smaller than the semiconducting gap)

$$\widetilde{n}_{\boldsymbol{k}}^{11} + \widetilde{n}_{\boldsymbol{k}}^{22} - 1 \approx \frac{{E_{\boldsymbol{k}}}^2 + \Gamma^2}{{E_{\boldsymbol{k}}}^2 + \Gamma^2 + \frac{|\Delta|^2}{\gamma_1 \gamma_2}} \, \frac{\gamma_1 - \gamma_2}{4\gamma_1\gamma_2} \, \frac{\Omega^2}{\epsilon_{\boldsymbol{k}}^2 + \Gamma^2} \, . \tag{14}$$

B. Self-Consistency Equation

We now solve self-consistently for the superconducting gap. The pairing part of the mean-field Hamiltonian originates from a microscopic Hamiltonian which involves a density-density type of interaction between the electrons in the semiconductor. The mean-field decoupling for this microscopic interaction of strength V (in a system of volume $\mathcal{V}$) is given by:

$$H_{e-e} \;=\; \frac{1}{\mathcal{V}} \sum_{\boldsymbol{k},\boldsymbol{k}'} V \; {c_{\mathbf{k}}^2}^{\dagger} \, {c_{-\mathbf{k}}^1}^{\dagger} \; c_{\mathbf{k}'}^1 \, c_{-\mathbf{k}'}^2 \tag{15}$$

$$\rightarrow \; \sum_{\boldsymbol{k}} \left(\Delta \; {c_{\mathbf{k}}^2}^{\dagger} \, {c_{-\mathbf{k}}^1}^{\dagger} + \Delta^* \; c_{\mathbf{k}}^1 \, c_{-\mathbf{k}}^2 \right) \, , \tag{16}$$

with

$$\Delta^* = \frac{1}{\mathcal{V}} \sum_{\boldsymbol{k}} V \langle {c_{\mathbf{k}}^2}^{\dagger} \, {c_{-\mathbf{k}}^1}^{\dagger} \rangle \xrightarrow[\mathcal{V}\to\infty]{} \int (\mathrm{d}\boldsymbol{k}) \; V \langle {c_{\mathbf{k}}^2}^{\dagger} {c_{-\mathbf{k}}^1}^{\dagger} \rangle \, , \tag{17}$$

where we wrote $(\mathrm{d}\boldsymbol{k}) \equiv \mathrm{d}^d\boldsymbol{k}/(2\pi)^d$ to shorten notations.

Eq. (17) is solved self-consistently by using the anomalous correlator in Eq. (10). The correct self-consistent condition involves only the real part of Eq. (10); this assertion will be justified in Sect. IV where we properly obtain the self-consistency relation from a saddle point condition (notice that this is trivially true in the limit $\Gamma \to 0$). More precisely we use the self consistency relation:

$$\Delta^* = \int (\mathrm{d}\boldsymbol{k}) \; V \tilde{s}_{\boldsymbol{k}}^{21} \, Re \left(\frac{1}{E_{\boldsymbol{k}} + i\Gamma} \right) \cdot (E_{\boldsymbol{k}} + i\Gamma) \tag{18}$$

We derive this rigorously in Sect. IV. Assuming that $\Omega \gg \Gamma$ and using Eq. (13) for the populations, the resulting gap equation reads

$$\begin{aligned} 1 &= -V \int (\mathrm{d}\boldsymbol{k})\, \frac{E_{\boldsymbol{k}}}{E_{\boldsymbol{k}}^2 + \Gamma^2 + 4\,|\Delta|^2}\, (\gamma_1 - \gamma_2) \\ &= -N_0 V\, (\gamma_1 - \gamma_2) \int_{-\Omega}^{\Omega} \mathrm{d}\epsilon\, \frac{E(\epsilon)}{E^2(\epsilon) + 4|\Delta|^2 + \Gamma^2}\ , \end{aligned} \tag{19}$$

with $N_0 \equiv \int (\mathrm{d}\boldsymbol{k})\, \delta(\epsilon_{\boldsymbol{k}})$ the density of states near the resonance.

Below, we study the solutions of the self-consistent equation in a few relevant cases.

1. *Bands with opposite velocities at resonance*

This is a very favorable case, so let us start with it. On the resonant surface $\mathcal{S}_{\omega_0}$, the dispersion relations of both bands can be Taylor-expanded as $\widetilde{E}_{1,2} = v_{1,2}\, q_\perp + \kappa_{1,2}\, q_\perp^2 + \ldots$, where $q_\perp$ is the momentum perpendicular to $\mathcal{S}_{\omega_0}$. So $\epsilon = v_-\, q_\perp + \kappa_-\, q_\perp^2 + \ldots$ and $E = v_+\, q_\perp + \kappa_+\, q_\perp^2 + \ldots$, where $v_\pm \equiv v_2 \pm v_1$ and $\kappa_\pm \equiv \kappa_2 \pm \kappa_1$. If the velocities are opposite in the two bands, *i.e.* $v_+ = 0$, one can express $E(\epsilon) \approx (\kappa_+/v_-^2)\, \epsilon^2$. Upon using this $E(\epsilon)$ in Eq. (19) and extending the limits of integration in Eq. (19) to $\pm\infty$ (for large Ω), we obtain

$$1 = -\frac{\pi}{\sqrt{2}} N_0 V\, \frac{|v_-|\, \mathrm{sgn}\, \kappa_+}{\sqrt{|\kappa_+|}}\, \frac{\gamma_1 - \gamma_2}{(4|\Delta|^2 + \Gamma^2)^{1/4}}\ . \tag{20}$$

We note that to get exact results in Eqs. (10) and (11). Notice that this equation can be satisfied for *both attractive or repulsive interactions* depending on the relative signs of $\gamma_1 - \gamma_2$ and of κ_+. Superconductivity is possible if the sign of V satisfies

$$\mathrm{sgn}\, V = \mathrm{sgn}(\gamma_2 - \gamma_1) \times \mathrm{sgn}\, \kappa_+\ , \tag{21}$$

and its magnitude satisfies the threshold condition

$$|V| \geq V_\mathrm{c} \equiv \frac{\sqrt{2}}{\pi} \frac{1}{N_0} \frac{\sqrt{|\kappa_+|}}{|v_-|} \frac{\sqrt{\Gamma}}{|\gamma_1 - \gamma_2|}\ . \tag{22}$$

This expresses the fact that superconductivity is favored by small and different decay rates.

If the conditions in Eqs. (21) and (22) are met, the superconducting gap is given by

$$|\Delta| = \frac{\Gamma}{2} \sqrt{\left(\frac{V}{V_\mathrm{c}}\right)^4 - 1}\ . \tag{23}$$

For large coupling constant, the gap scales as the square of the interaction strength V. Notice also that the gap does not vanish in the limit $\Gamma \to 0$ because the threshold disappears simultaneously. In this limit,

$$|\Delta| \xrightarrow[\Gamma \to 0]{} \frac{\pi^2}{4}\, (N_0 V)^2\, \frac{v_-^2}{|\kappa_+|}\, (\gamma_1 - \gamma_2)^2\ . \tag{24}$$

Robustness. Let us examine the domain of validity of our results. Let us first argue that the condition $v_+ = 0$ that we used above can be achieved by a proper choice of the laser frequency ω_0. In practice, one may proceed as follows. The resonance surface $\mathcal{S}_{\omega_0}$ can be swept as one changes ω_0. At $\boldsymbol{k}_0 \in \mathcal{S}_{\omega_0}$, $\epsilon_{\boldsymbol{k}_0} = 0$ by definition. Assume for simplicity a spherical-symmetric dispersion. As one scans ω_0, one should search for the frequency for which $E_{\boldsymbol{k}_0}$ reaches an extremum, either a minimum or maximum. The extremum would correspond to a zero of v_+. Finding the extremum condition may require using higher and lower bands; we illustrate this for a few examples of band structure topologies in Fig. (3). By changing the chemical potential, one can make the value of the extremum be zero, *i.e.* $E_{\boldsymbol{k}_0} = 0$, and therefore $E(\epsilon) \propto \epsilon^2$.

Additionally, we note that our results are relatively stable in the case of a non-vanishing v_+. Indeed, our results are essentially unchanged as long as

$$|v_+| \leq \sqrt{|\kappa_+|\, \Gamma}\, \frac{|V|}{V_\mathrm{c}}\ . \tag{25}$$

Most importantly, our results are robust against finite temperatures of the reservoirs. Indeed, this corresponds to changes in $n_\mathrm{F}(E_1(\boldsymbol{k}))$ and $n_\mathrm{F}(E_2(\boldsymbol{k}))$ which may be neglected for temperatures less then the semiconducting gap E_g.

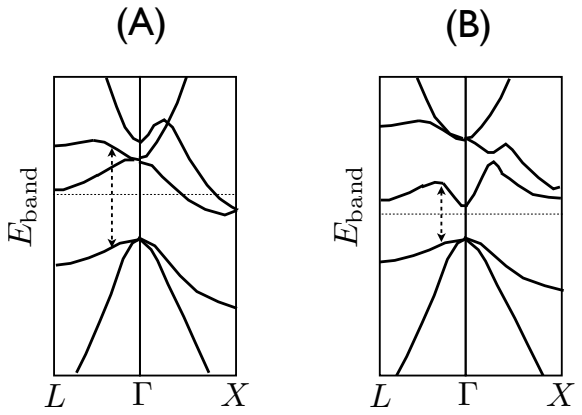

FIG. 3: Examples of how to choose optimal conditions. One must seek points in the Brillouin zone where two bands have opposite velocities. The transitions are depicted by the vertical dashed line, whose length determines the laser frequency ω_0. Notice that the transition of choice does not need to be between two consecutive bands, as is the case depicted in (A). In (B), the transition of choice is between two consecutive bands. The horizontal dashed line demarcates the position of the chemical potential, which can be chosen by doping or gating. The topologies of the band structures were sketched to resemble the bands in Si (A) and in GaAs (B).

2. Weak Rabi frequency

Previously we considered the case in which the laser Rabi frequency Ω was large compared to the decay rate Γ. This condition is most favorable towards superconducting pairing; however for many systems it is not satisfied. For lasers with moderate power (say on the order of milliwatts) and semiconductors at room temperatures, the laser Rabi frequency is several hundred megahertz while the carrier decay rate is several tens of gigahertz. It is therefore relevant to repeat the previous analysis in the less favorable case in which the Rabi frequency is less than the particle decay rate.

Following the steps of Sect. II B 1, but using here the non-equilibrium population deviation given in Eq. (14), the superconducting self-consistency equation now reads

$$1 = -\frac{\pi}{4\sqrt{2}} N_0 V \frac{|v_-| \operatorname{sgn}\kappa_+ \sqrt{|\kappa_+|}}{v_-^2 \sqrt{|\Delta|^2 + \gamma_1\gamma_2\Gamma^2} + \sqrt{\gamma_1\gamma_2}\Gamma^2 |\kappa_+|} \times \frac{1}{(\gamma_1\gamma_2)^{1/4}} \frac{\gamma_1 - \gamma_2}{\left(|\Delta|^2 + \gamma_1\gamma_2\Gamma^2\right)^{1/4}} \Omega^2 \,. \tag{26}$$

We recover the previous condition on the sign of the electron-electron interaction, namely

$$\operatorname{sgn} V = \operatorname{sgn}(\gamma_2 - \gamma_1) \times \operatorname{sgn}\kappa_+ \,, \tag{27}$$

and the threshold condition now reads

$$|V| \geq V_c' \;\equiv\; \frac{4\sqrt{2}}{\pi} \frac{1}{N_0} \frac{v_-^2 + |\kappa_+|\Gamma}{|v_-|\sqrt{|\kappa_+|}} \frac{\gamma_1\gamma_2\,\Gamma^{3/2}}{|\gamma_1 - \gamma_2|} \frac{1}{\Omega^2}, \tag{28}$$

Compared to the case $\Omega \gg \Gamma$ [see Eq. (22)], the threshold condition has changed by a factor $4\gamma_1\gamma_2(\Gamma^2/\Omega^2) \times [|\kappa_+|\,\Gamma/(|v_-|^2 + \Gamma\,|\kappa_+|)]$. We note that, while in this case both factors Γ^2/Ω^2 and $|\kappa_+|\,\Gamma/(|v_-|^2 + \Gamma\,|\kappa_+|)$ increase the

threshold, this could be compensated if the two bands have rather different decay rates, in which case the factor $\gamma_1\gamma_2$ can be small. If both conditions in Eqs. (27) and (28) are met and $|v_-|^2 \gg |\kappa_+|\,\Gamma$, the gap is then given by

$$|\Delta| = \Gamma\,\sqrt{\gamma_1\gamma_2}\,\sqrt{\left(\frac{|V|}{V_c'}\right)^{4/3} - 1}\,. \tag{29}$$

Note that for large electronic interactions $|V|$, the gap is linear in the decay rate Γ.

Vanishing decay rates. One particularly interesting case is when the Rabi frequency is small but the two decay rates Γ_1 and Γ_2 are very different so that $\gamma_1\gamma_2 \approx 0$. Repeating the previous steps, the superconducting self-consistency equation reads

$$\begin{aligned} 1 =& \frac{\pi}{\sqrt{2}} N_0 V\,(\gamma_2 - \gamma_1)\,\Omega \\ &\times \frac{|v_-|\,\mathrm{sgn}\,\kappa_+}{\left[\Omega^2\,|\kappa_+|^2\,\Gamma^2(4|\Delta|^2 + \Omega^2)\right]^{1/4} + 2\,|v_-|\,|\Delta|} \end{aligned} \tag{30}$$

yielding the condition

$$\mathrm{sgn}\,V = \mathrm{sgn}(\gamma_2 - \gamma_1) \times \mathrm{sgn}\,\kappa_+\,, \tag{31}$$

and the threshold

$$|V| \geq V_c'' \equiv \frac{\sqrt{2}}{\pi}\,\frac{1}{N_0}\,\frac{\sqrt{|\kappa_+|}}{|v_-|}\,\frac{\Gamma}{|\gamma_1 - \gamma_2|}\,. \tag{32}$$

We note that this is the same threshold as in Eq. (22) where we considered the case of a large Rabi frequency $\Omega \gg \Gamma$. Whenever this threshold is satisfied in the case of a large $|v_-|$, the superconducting order parameter reads

$$|\Delta| = \frac{\Omega}{2}\,\frac{\sqrt{\Gamma|\kappa_+|}}{|v_-|}\left(\frac{|V|}{V_c''} - 1\right)\,. \tag{33}$$

C. Dynamics of the order parameter

We now confirm our analytic predictions by numeric integration of the equations of motion, see Eqs. (9a), (9b), (9c) and (9d). We start by briefly describing our numerical simulation procedure. For simplicity we consider the case when the $E_\alpha(\boldsymbol{k})$ are spherically symmetric. Furthermore by focusing on the region near the resonant surface $\mathcal{S}_{\omega_0}$ we may ignore variations in the density of states. In this case, within mean field, we may reduce the dynamics of the 3-d model to the dynamics of an equivalent one dimensional model where for simplicity we can mathematically shift the surface $\mathcal{S}_{\omega_0}$ to the wavevector $\boldsymbol{k}_0 = 0$. Furthermore we will assume that $\widetilde{E}_{1,2} = v_{1,2}\,k + \kappa_{1,2}\,k^2$ (with no higher order corrections). We will assume that $\kappa_- = v_+ = 0$ and the density of states is set to $N_0 = 1/2\pi$. We also scale all units such that all quantities become dimensionless. We consider an initial state ($t = 0$) where the populations and coherences are initialized at their zero-temperature equilibrium values $\widetilde{n}^{21}_{\boldsymbol{k}} = 0$, $\widetilde{n}^{11}_{\boldsymbol{k}} = n_F\,(E_1(\boldsymbol{k}))$ and $\widetilde{n}^{22}_{\boldsymbol{k}} = n_F\,(E_2(\boldsymbol{k}))$. The superconducting correlations are initialized at a very small but non-zero value $\widetilde{s}^{21}_{\boldsymbol{k}} = 0.02\cdot\widetilde{s}^{21}_{\boldsymbol{k},Eq}$ where $\widetilde{s}^{21}_{\boldsymbol{k},Eq}$ is the steady state anomalous correlator as computed in Sect. II (we also considered random initial conditions and obtained similar results). We then time evolve the equations (9a), (9b), (9c) and (9d) until we reach a steady state. We have used the self-consistency relation in Eq. (18). In Fig. 4, we present our numeric simulations for three representative coupling constants (where $\Omega \gg \Gamma$ and $\gamma_1 \gg \gamma_2$). In Fig. 4(a), we plot the superconducting gap as a function of time: it converges to the order parameter theoretically predicted in Eq. (23). To get good matching we have calculated the correction to Eq. (23) due to the finite cutoff in k-space $|k_{\max}| = 0.2$ used in the numerical simulations. In Fig. 4(b) we plot the theoretically predicted values of the anomalous correlator $\widetilde{s}^{21}_{\boldsymbol{k}}$ as a function of $\boldsymbol{k}$. We generate $\widetilde{s}^{21}_{\boldsymbol{k}}$ in two different ways: one using the theoretical predictions for the steady state given in Eqs. (10) and (11) and using the value of $|\Delta|$ from the simulations and also using the final values of the anomalous correlators $\widetilde{s}^{21}_{\boldsymbol{k}}$ as computed from the numerical integrations. The agreement is excellent.

To show that our theory is able to predict superconducting pairing even when our approximations for $\widetilde{n}^{11}_{\boldsymbol{k}} + \widetilde{n}^{22}_{\boldsymbol{k}} - 1$ and hence $\widetilde{s}^{21}_{\boldsymbol{k}}$ are not accurate, see Eq. (13), we have chosen parameters outside the approximations of Sect. II B. One way to make these approximations inaccurate is to consider a value of $\gamma_1, \gamma_2 \succeq \frac{\Omega^2}{\Gamma^2 + |v_-|^2\Gamma/\kappa_+}$ see the discussion below

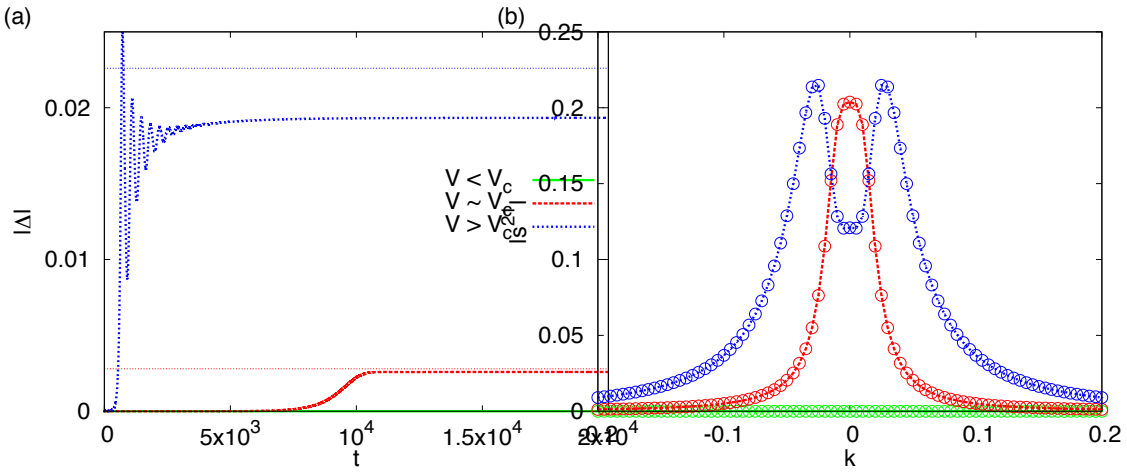

FIG. 4: (a) Time evolution of the order parameter Δ for three representative values of the coupling constant: $V = 5 > V_c = 2.14$, $V = 2.3 \sim V_c$ and $V = 1 < V_c$. The straight lines correspond to the analytic expressions in Eq. (23). Here V_c is computed using Eq. (22) (corrected to account for cutoff effects). (b) Perfect matching between the steady-state anomalous correlator $\widetilde{s}^{21}_{\boldsymbol{k}}$ as given by Eq. (10) (straight lines) and the anomalous correlator $\widetilde{s}^{21}_{\boldsymbol{k}}$ obtained numerically after the time dynamics have converged (circles). The color coding is the same as in (a). ($\kappa_+ = -50$, $v_- = 10$, $\Omega = 0.5$, $\Gamma = 10^{-2}$ and $\gamma_2 = 10^{-3}$).

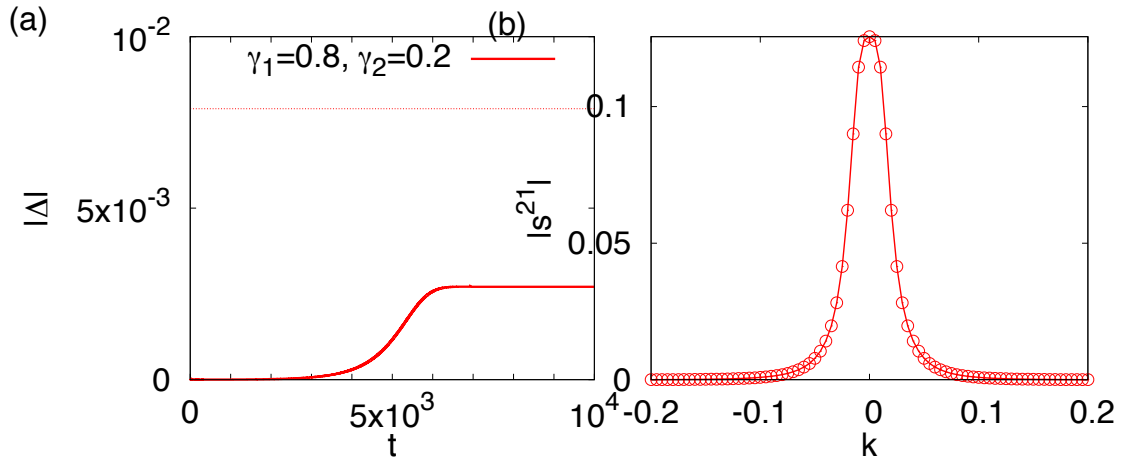

FIG. 5: (a) Time evolution of the superconducting pairing Δ for a scenario where $\gamma_1 \sim \gamma_2$. The straight line corresponds to the steady-state value computed with Eq. (23). The discrepancy between analytics and numerics is because the parameters for the numeric integration are outside the limits of the approximations used in Sect. II B. (b) Perfect matching between the steady-state anomalous correlator $\widetilde{s}^{21}_{\boldsymbol{k}}$ as given by Eq. (10) (straight lines) and the anomalous correlator $\widetilde{s}^{21}_{\boldsymbol{k}}$ obtained numerically after the time dynamics have converged (circles). ($\kappa_+ = -50$, $v_- = 10$, $\Omega = 0.5$, $\Gamma = 10^{-2}$, $\gamma_1 = 0.8$ and $V = 5$).

Eq. (13). In Fig. 5 (a), we have plotted the value of $|\Delta|$ as a function of time, we see that despite the failure of Eq. (13) we still obtain a relatively strong superconducting paring within a factor of three of the analytical one. We also have compared the In Fig. 5 (b) we plot the theoretically predicted values of the anomalous correlator $\widetilde{s}^{21}_{\boldsymbol{k}}$ as a function of $\boldsymbol{k}$. We generate $\widetilde{s}^{21}_{\boldsymbol{k}}$ in two different ways: one using the theoretical predictions for the steady state given in Eqs. (10) and (11) and the value of $|\Delta|$ from the simulations and also using the final values of the anomalous correlators $\widetilde{s}^{21}_{\boldsymbol{k}}$ as computed from the numerical integrations. The agreement is excellent. We conclude that the system also reaches a non-trivial steady state for parameter ranges outside the validity of the approximations used in Sect. II B.

We have also numerically verified that it is possible to obtain superconductivity for the case when $\Omega < \Gamma$. We have numerically integrated the time evolution of the order parameter for two such values of Ω and Γ. We chose $\gamma_1\gamma_2 \sim 0$ in order to have a non-zero order parameter (see the discussion in Sect. II B 2). We see that the order parameter develops but the time evolution is highly oscillatory and the time scale for convergence is increased by ~ 100. This is because one of the decay rates, Γ_2, is very small so it takes a long time for the oscillations to decay.

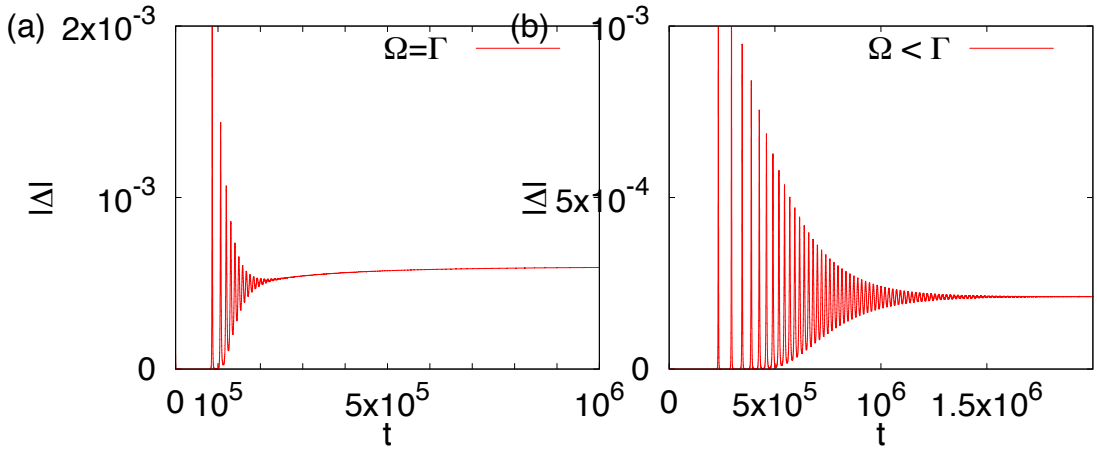

FIG. 6: (a) Time evolution of the order parameter Δ for $\Omega = \Gamma = 10^{-2}$. (b) Time evolution of the order parameter Δ for $\Omega = \Gamma/5 = 0.2\,10^{-2}$. ($\kappa_+ = -50$, $v_- = 10$, $\Gamma = 10^{-2}$, $\gamma_2 = 10^{-4}$, $V = 20$).

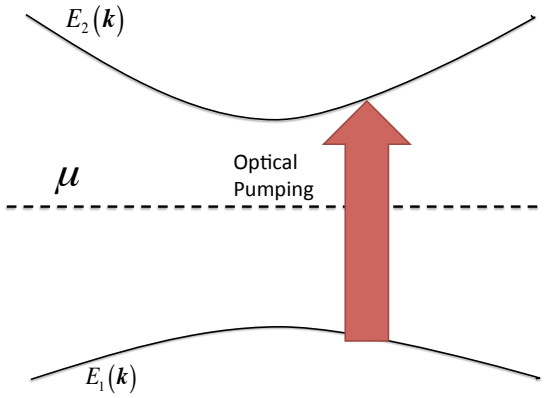

FIG. 7: Optical pumping. The upper band (1) of a two-band semiconductor is populated with a single broad band optical pump. The chemical potential μ is tuned halfway between the two bands.

III. OPTICAL PUMPING OF A TWO-BAND SEMICONDUCTOR

Let us now turn to an alternate scenario, which may be more easily realized in the lab. Let us consider a two-band semiconductor model whose population of the bottom band is optically pumped into the upper band *via* a *broad band* light source and whose interband relaxation is slow, *e.g.* negligible optical phonon coupling. The lower band ($\alpha = 1$) with dispersion $E_1(\boldsymbol{k})$ and the upper band ($\alpha = 2$) with dispersion $E_2(\boldsymbol{k})$ are separated by a gap $E_{\rm g}$.

In order to reach a non-trivial steady state, the coupling to a thermal reservoir is necessary to drain the energy which is continuously injected in the system. However, unlike the previous case, the reservoir does not need to play the role of an extra "storage" of particles (or holes) and a single weakly-coupled reservoir is enough. We set the chemical potential μ in the gap, see Fig. (7), such that there are momenta $\boldsymbol{k}_0$ lying on a closed surface $\mathcal{S}$ of the Brillouin zone where the condition $E_1(\boldsymbol{k}_0) + E_2(-\boldsymbol{k}_0) = 0$ is satisfied. Here, μ corresponds to the field produced by the external voltages (say set by external gates). We do not assume that $E_\alpha(\boldsymbol{k}_0) = \text{const}$. We shall also assume the the optical pumping laser (or broadband source) is not on resonance with these momenta $\boldsymbol{k}_0$.

Neglecting superconductivity temporarily, the main effect of the optical pumping is to modify the population of the lower and upper bands to some non-trivial distribution. Since the pumping and the interband relaxation is weak, the populations of the two bands relax to a separate quasi-thermal equilibrium within each band. Therefore, the bands can effectively be seen as having two different chemical potentials μ_1 and μ_2[26]. We note that μ_1 and μ_2 are not directly related to the energy levels of the Hamiltonian describing the semiconductor. They can be seen as the Lagrange multipliers enforcing the average number of particles in the two bands and depend on the balance between

the strength of the drive and the inter-band relaxation. Once the system is quasi-equilibrated, we may write

$$\begin{aligned} n_{\boldsymbol{k}}^{11} &= n_{\mathrm{F}}\left(E_1\left(\boldsymbol{k}\right),\mu_1\right) \ , \\ n_{-\boldsymbol{k}}^{22} &= n_{\mathrm{F}}\left(E_2\left(-\boldsymbol{k}\right),\mu_2\right) \ , \\ n_{\boldsymbol{k}}^{12} &= 0 \ . \end{aligned} \tag{34}$$

Here, $n_{\mathrm{F}}\left(\epsilon,\mu\right) \equiv \left[1+\exp\left(\left(\epsilon-\mu\right)/T\right)\right]^{-1}$ is the Fermi-Dirac distribution and T is the temperature of the underlying crystal. The equations of motion for the populations and anomalous correlators which are consistent with the steady state given in Eqs. (34) read:

$$\begin{aligned} \frac{\mathrm{d}}{\mathrm{d}t}n_{\boldsymbol{k}}^{11} =& \mathrm{i}\Delta s_{\boldsymbol{k}}^{21} - \mathrm{i}\Delta^* s_{\boldsymbol{k}}^{21*} - 2\Gamma_1\left(\boldsymbol{k}\right)\tilde{n}_{\boldsymbol{k}}^{1} \\ \frac{\mathrm{d}}{\mathrm{d}t}n_{-\boldsymbol{k}}^{22} =& \mathrm{i}\Delta s_{\boldsymbol{k}}^{21} - \mathrm{i}\Delta^* s_{\boldsymbol{k}}^{21*} - 2\Gamma_2\left(\boldsymbol{k}\right)\tilde{n}_{-\boldsymbol{k}}^{2} \\ \frac{\mathrm{d}}{\mathrm{d}t}s_{\boldsymbol{k}}^{21} =& \mathrm{i}\left(E_{\boldsymbol{k}}\left(\boldsymbol{k}\right) - \mathrm{i}\Gamma_{21}\left(\boldsymbol{k}\right)\right)s_{\boldsymbol{k}}^{21} + \mathrm{i}\Delta^*\left(n_{\boldsymbol{k}}^{11} + n_{-\boldsymbol{k}}^{22} - 1\right) \end{aligned} \tag{35}$$

Here, $E_{\boldsymbol{k}} \equiv E_1\left(\boldsymbol{k}\right) + E_2\left(\boldsymbol{k}\right)$ and $\tilde{n}_{\boldsymbol{k}}^{\alpha} \equiv \left[n_{\boldsymbol{k}}^{\alpha\alpha} - n_F\left(E_\alpha\left(\boldsymbol{k}\right),\mu_\alpha\right)\right]$. Γ_α are the relaxation rates for the two bands and Γ_{12} is the superconducting decay rate. In principle, these can be obtained by linearizing the Boltzmann equation (collision integral) close to equilibrium. Typically, $\Gamma_{12} \propto \Gamma_1 + {\Gamma_2}$[26]. We also drop the $\boldsymbol{k}$ dependence of Γ since we are only considering a small portion of the Brillouin zone near the surface $\mathcal{S}$. The steady-state solution of these equations reads

$$s_{\boldsymbol{k}}^{21} = -\frac{\Delta^*}{E_{\boldsymbol{k}} + \mathrm{i}\Gamma_{12}}\ \left(n_{\boldsymbol{k}}^{11} + n_{-\boldsymbol{k}}^{22} - 1\right) \tag{36}$$

and

$$\begin{aligned} n_{\boldsymbol{k}}^{11} + n_{-\boldsymbol{k}}^{22} - 1 =& \frac{1}{\Xi'}\ 4\gamma_1\gamma_2\ \left(\Gamma/\Gamma_{12}\right)^2 \\ & \times\left[n_{\mathrm{F}}\left(E_1(\boldsymbol{k}),\mu_1\right) + n_{\mathrm{F}}\left(E_2(-\boldsymbol{k}),\mu_2\right) - 1\right], \end{aligned} \tag{37}$$

where we defined

$$\Xi' \equiv 4\gamma_1\gamma_2\left(\Gamma/\Gamma_{12}\right)^2 + \frac{4|\Delta|^2}{{E_{\boldsymbol{k}}}^2 + \Gamma_{12}^2}\ . \tag{38}$$

Other pumping schemes If other bands are present, other pumping schemes can be considered. For instance, a third band can be used to either populate or depopulate the two other bands, see Fig. (8). We note that with these pumping schemes we can choose the sign of the population deviation $n_{\boldsymbol{k}}^{11} - n_{-\boldsymbol{k}}^{22} - 1$. Also, our method is likely to work with carrier injection pumping[27]. The conclusions presented in this Section apply just as well for these generalized scenarios.

A. Self-consistency equation

We now solve self-consistently for the superconducting gap. The pairing part of the mean-field Hamiltonian originates from a microscopic Hamiltonian which involves a density-density type of interaction between the electrons in the semiconductor. The mean-field decoupling for this microscopic interaction of strength V (in a system of volume $\mathcal{V}$) is given by:

$$\begin{aligned} H_{e-e} \ &= \ \frac{1}{\mathcal{V}}\sum_{\boldsymbol{k},\boldsymbol{k'}} V\ {c_{\mathbf{k}}^{2}}^{\dagger}\,{c_{-\mathbf{k}}^{1}}^{\dagger}\ c_{\mathbf{k'}}^{1}\,c_{-\mathbf{k'}}^{2} \\ &\rightarrow\ \sum_{\boldsymbol{k}}\left(\Delta\ {c_{\mathbf{k}}^{2}}^{\dagger}\,{c_{-\mathbf{k}}^{1}}^{\dagger} + \Delta^*\ c_{\mathbf{k}}^{1}\,c_{-\mathbf{k}}^{2}\right)\ , \end{aligned} \tag{39}$$

with

$$\Delta^* = \frac{1}{\mathcal{V}}\sum_{\boldsymbol{k}} V\langle {c_{\mathbf{k}}^{2}}^{\dagger}\,{c_{-\mathbf{k}}^{1}}^{\dagger}\rangle \xrightarrow[\mathcal{V}\rightarrow\infty]{} \int(\mathrm{d}\boldsymbol{k})V\langle {c_{\mathbf{k}}^{2}}^{\dagger}\,{c_{-\mathbf{k}}^{1}}^{\dagger}\rangle\ , \tag{40}$$

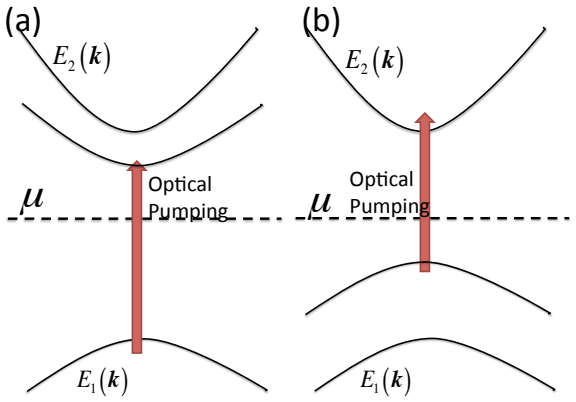

FIG. 8: Different available optical pumping mechanisms in a three band semiconductor. (a) Deplete the population of the bottom band into a third reservoir band. (b) Populate the top band from a third band.

where we wrote $(\mathrm{d}\boldsymbol{k}) \equiv \mathrm{d}^d\boldsymbol{k}/(2\pi)^d$ to shorten notations.

We solve for the self-consistent condition Eq. (40) using the anomalous correlator in Eq. (36). The correct self-consistent condition involves only the real part of Eq. (36); this assertion will be justified in Sect IV where we properly obtain the self-consistency relation from a saddle point condition (notice that this is trivially true in the limit $\Gamma \to 0$). The resulting gap equation is

$$\begin{aligned} 1 \;=\; -V \int (\mathrm{d}\boldsymbol{k})\, & \frac{\gamma_1\gamma_2\,(\Gamma/\Gamma_{12})^2\, E_{\boldsymbol{k}}}{\gamma_1\gamma_2\,(\Gamma/\Gamma_{12})^2\,(E_{\boldsymbol{k}}^2+\Gamma_{12}^2)+|\Delta|^2} \\ & \times \left[n_{\mathrm{F}}\left(E_1(\boldsymbol{k}),\mu_1\right)+n_{\mathrm{F}}\left(E_2(-\boldsymbol{k}),\mu_2\right)-1\right]\,. \end{aligned} \tag{41}$$

Let us now study the solutions of the self-consistent equation (41) by first focusing on the very favorable case in which the two bands have opposite velocities. On the resonant surface $\mathcal{S}$, where $E_1(\boldsymbol{k})+E_2\,(-\boldsymbol{k})=0$, the dispersion relations can be Taylor-expanded as $\widetilde{E}_{1,2}=v_{1,2}\,q_\perp+\kappa_{1,2}\,q_\perp^2+\ldots$, where $q_\perp$ is the momentum perpendicular to the resonant surface $\mathcal{S}$. So $E=v_+\,q_\perp+\kappa_+\,q_\perp^2+\ldots$, where $v_\pm=v_2\pm v_1$ and $\kappa_\pm=\kappa_2\pm\kappa_1$. When the velocities are opposite in the two bands, *i.e.* $v_+=0$, one can express $E(\epsilon)\approx(\kappa_+/v_-^2)\,\epsilon^2$. Upon using this $E(\epsilon)$ in Eq. (41) and extending the limits of integration to $\pm\infty$, we obtain:

$$\begin{aligned} 1 = -\frac{\pi}{\sqrt{2}}N_0V\,\frac{|v_-|\,\mathrm{sgn}\,\kappa_+}{\sqrt{|\kappa_+|}}\,(\gamma_1\gamma_2)^{1/4}\,(\Gamma/\Gamma_{12})^{1/2} \\ \times\,\frac{\left[n_{\mathrm{F}}\left(E_1(\boldsymbol{k}),\mu_1\right)+n_{\mathrm{F}}\left(E_2(-\boldsymbol{k}),\mu_2\right)-1\right]}{(|\Delta|^2+\gamma_1\gamma_2\Gamma^2)^{1/4}}\,. \end{aligned} \tag{42}$$

Here N_0 is the density of states at $\mathcal{S}$. We note that in the case where κ_+ is not uniform over the surface $\mathcal{S}$ we can replace $\sqrt{|\kappa_+|}$ in the equation above by its average to obtain the correct results for this case. We will not consider this extension further. Notice that this equation can be satisfied for *both attractive or repulsive interactions* depending on the relative signs of $n_{\mathrm{F}}\left(E_1(\boldsymbol{k}),\mu_1\right)+n_{\mathrm{F}}\left(E_2(-\boldsymbol{k}),\mu_1\right)-1$ and of κ_+. Superconductivity is possible if the sign of V satisfies

$$\begin{aligned} \mathrm{sgn}\,V = & -\mathrm{sgn}\,\kappa_+ \\ & \times\,\mathrm{sgn}\left[n_{\mathrm{F}}\left(\left(E_1(\boldsymbol{k}),\mu_1\right)+n_{\mathrm{F}}\left(E_2(-\boldsymbol{k}),\mu_2\right)-1\right]\,, \end{aligned} \tag{43}$$

and if its magnitude satisfies the threshold condition

$$|V| \geq V_{\mathrm{c}}''' \equiv \frac{\sqrt{2}}{\pi}\frac{1}{N_0}\frac{\sqrt{|\kappa_+|}}{\mathrm{N}|v_-|}\sqrt{\Gamma_{12}}\,. \tag{44}$$

Here $\mathrm{N} \equiv n_{\mathrm{F}}\left(E_1(\boldsymbol{k}),\mu_1\right)+n_{\mathrm{F}}\left(E_2(-\boldsymbol{k}),\mu_2\right)-1$. The condition in Eq. (44) is very similar to the one obtained in Eq. (22). This expresses the fact that superconductivity is favored by small decay rates, *e.g.* weak coupling to longitudinal phonons and impurities.

If the conditions in Eqs. (43) and (44) are met, the superconducting gap is given by

$$|\Delta| = \sqrt{\gamma_1 \gamma_2}\, \Gamma \sqrt{\left(\frac{V}{V_{\rm c}'''}\right)^4 - 1}\,. \tag{45}$$

This corresponds to a robust gap that scales linearly with the decay rate Γ, and, for large coupling constant, scales as the square of the interaction strength V.

Robustness. Let us examine the domain of validity of the results we presented in this Section. First, we remark that they are relatively stable in the case v_+ is non-vanishing. Indeed, the results are essentially unchanged as long as

$$|v_+| \leq \sqrt{|\kappa_+|\,\Gamma}\,\frac{|V|}{V_{\rm c}'''}\,. \tag{46}$$

Therefore, the condition $v_+ = 0$ that we used above does not have to be perfectly tuned.

Most importantly, the results of these Section are stable to changes of temperature in the semiconductor. Indeed those would correspond to changes in $n_{\rm F}(E_1(\boldsymbol{k}))$ and $n_{\rm F}(E_2(\boldsymbol{k}))$ which may be neglected for temperatures less then the semiconducting gap $E_{\rm g}$. We note that in realistic setups, Γ may be temperature dependent.

IV. KELDYSH APPROACH

In this Section, we revisit the self-consistent mean-field condition for superconductivity that we used multiple times in the previous Sections. Starting from a particle conserving theory, we justify the approximation that we used to obtain Eqs. (19) and (41) which consisted in considering only the part of the anomalous correlator $s_{\boldsymbol{k}}^{\dagger 21}$ in phase with Δ^*. For the sake of simplicity, we concentrate on the case described in Sect. II. We derive a Keldysh mean-field theory for the laser-driven semiconductor system and solve for the symmetry-breaking order-parameter corresponding to the superconducting pairing. The full Keldysh action reads

$$S_{\rm K} = S_{e-e} + S_{\rm other} \tag{47a}$$

with

$$S_{e-e} = \int_\Upsilon {\rm d}t \int {\rm d}^d\boldsymbol{r}\; V\; \bar{\Phi}\left(\boldsymbol{r},t\right) \Phi\left(\boldsymbol{r},t\right)\;, \tag{47b}$$

where $\Phi(\boldsymbol{r},t) \equiv c^1(\boldsymbol{r},t)\, c^2(\boldsymbol{r},t)$, $\bar{\Phi}(\boldsymbol{r},t) = c^{2\dagger}(\boldsymbol{r},t) c^{1\dagger}(\boldsymbol{r},t)$, V is the coupling strength and $S_{\rm other}$ is the quadratic action corresponding to all the other terms in the Hamiltonian (1) such as $c^1_{\boldsymbol{k}}$, $c^2_{\boldsymbol{k}}$, $a^1_{\boldsymbol{k},n}$ and $a^2_{\boldsymbol{k},n}$. Υ is the Keldysh contour which goes forward from time minus infinity to plus infinity and then backward. We now perform a Hubbard-Stratonovich transformation in S_{e-e} so as to obtain

$$\exp\left[{\rm i}\int_\Upsilon {\rm d}t \int {\rm d}^d\boldsymbol{r}\; V\; \bar{\Phi}\left(\boldsymbol{r},t\right) \Phi\left(\boldsymbol{r},t\right)\right] = \int \mathcal{D}[\Delta]\;\; {\rm e}^{{\rm i}\int_\Upsilon {\rm d}t \int {\rm d}^d\boldsymbol{r}\, \left[-\frac{1}{V}|\Delta(\boldsymbol{r},t)|^2 + \Delta(\boldsymbol{r},t)\,\bar{\Phi}(\boldsymbol{r},t) + \Delta^*(\boldsymbol{r},t)\,\Phi(\boldsymbol{r},t)\right]}\,. \tag{48}$$

Integrating out all the fields in $S_{\rm K}$ except for Δ, we obtain an effective action for $\Delta\left(\boldsymbol{r},t\right)$ and the zero-source generating functional reads

$$Z = \int \mathcal{D}[\Delta^+,\Delta^-]\;\; {\rm e}^{{\rm i}S_{\rm eff}[\Delta^+,\Delta^-]}\,, \tag{49}$$

with the effective action expressed in terms of the fields Δ^+ and Δ^- which correspond to the order-parameter in the forward and backward branch of the Keldysh contour

$$\begin{aligned} S_{\rm eff}[\Delta^+,\Delta^-] \equiv & \widetilde{S}[\Delta^+,\Delta^-] \\ & - \frac{1}{V}\int {\rm d}t{\rm d}^d\boldsymbol{r}\left(|\Delta^+(\boldsymbol{r},t)|^2 - |\Delta^-(\boldsymbol{r},t)|^2\right). \end{aligned} \tag{50}$$

$\widetilde{S}[\Delta^+,\Delta^-]$ can be computed through a series of Feynman diagrams as represented in Fig. (9). The propagators for these diagrams are those that make for the action $S_{\rm other}$. Given that $S_{\rm other}$ is Gaussian, we use Wick's theorem to calculate those Feynman diagrams.

We solve for the saddle point of the effective action by focusing on the solutions that are homogeneous in time and space. We write $\Delta^{\pm} = \Delta \pm \delta$, and note that the effective action vanishes for $\delta = 0$ for any Δ. This is a general result that stems from the fact that for classical field configurations, the action on the backward branch is canceled exactly by that of the forward branch. Thus, the variation of the effective action with respect to Δ vanish for fixed $\delta = 0$. The condition that determines Δ at the saddle, is obtained by varying the action with respect to δ: expanding the action in powers of δ, the saddle point condition is that the terms linear in δ vanish. These terms can be collected in perturbation theory.

Expanding $S_{\rm eff}[\Delta, \delta]$, we observe that all the terms contain $\delta\Delta^*$, $\delta^*\Delta$, and powers of $|\Delta|^2$. The action is invariant under simultaneous phase rotations of δ and Δ. So we can fix the phase of δ to be zero, *i.e.* make δ real (this is, of course, a gauge choice for the fermionic description of the problem). All terms linear in δ are multiplying the combination $(\Delta + \Delta^*)$ and powers of $|\Delta|^2$. Factoring out this combination $\delta(\Delta + \Delta^*)$ in the expansion of $S_{\rm eff}[\Delta, \delta]$ leads to an equation that depends only on $|\Delta|$. This equation determines the saddle point value for $|\Delta|$. We choose Δ to be real as well, and then simplify the saddle point search by considering both δ and Δ in phase and real. The net effect of this procedure is to neglect the relative phase fluctuations of Δ^+ and Δ^- – which are assumed to be small for a physical solution. The saddle point equation in this case becomes

$$0 = \partial_\delta \left[-\frac{4\delta\Delta}{V} + \widetilde{\mathcal{L}}\left[\Delta, \delta\right] \right]_{\delta=0} . \tag{51}$$

We compute $\partial_\delta \widetilde{\mathcal{L}}\left[\Delta, \delta\right]\big|_{\delta=0}$ by summing over the Feynman diagrams in Fig. (9) and obtain

$$\begin{aligned}
&\partial_\delta \widetilde{\mathcal{L}}\left[\Delta, \delta\right]\big|_{\delta=0} = \\
&\sum_{n=1}^{\infty} \left|\frac{\Delta}{2}\right|^{2n-1} \int (\mathrm{d}\boldsymbol{k}) \int \frac{\mathrm{d}\omega}{2\pi}\, \mathrm{Tr} \left\{ \begin{pmatrix} 0 & \mathbb{1} \\ \mathbb{1} & 0 \end{pmatrix} \left[\begin{pmatrix} G^R(\boldsymbol{k},\omega) & G^K(\boldsymbol{k},\omega) \\ 0 & G^A(\boldsymbol{k},\omega) \end{pmatrix} \begin{pmatrix} \mathrm{i}\sigma^y G^A(\boldsymbol{k},-\omega)\mathrm{i}\sigma^y & \mathrm{i}\sigma^y G^K(\boldsymbol{k},-\omega)\mathrm{i}\sigma^y \\ 0 & \mathrm{i}\sigma^y G^R(\boldsymbol{k},-\omega)\mathrm{i}\sigma^y \end{pmatrix} \right]^n \right\} \\
&+ \sum_{n=1}^{\infty} \left|\frac{\Delta}{2}\right|^{2n-1} \int (\mathrm{d}\boldsymbol{k}) \int \frac{\mathrm{d}\omega}{2\pi}\, \mathrm{Tr} \left\{ \begin{pmatrix} 0 & \mathbb{1} \\ \mathbb{1} & 0 \end{pmatrix} \left[\begin{pmatrix} \mathrm{i}\sigma^y G^A(\boldsymbol{k},-\omega)\mathrm{i}\sigma^y & \mathrm{i}\sigma^y G^K(\boldsymbol{k},-\omega)\mathrm{i}\sigma^y \\ 0 & \mathrm{i}\sigma^y G^R(\boldsymbol{k},-\omega)\mathrm{i}\sigma^y \end{pmatrix} \begin{pmatrix} G^R(\boldsymbol{k},\omega) & G^K(\boldsymbol{k},\omega) \\ 0 & G^A(\boldsymbol{k},\omega) \end{pmatrix} \right]^n \right\} .
\end{aligned} \tag{52}$$

Here $G^{A/R/K}$ stand for the advanced, retarded and Keldysh components of the electronic Green's functions for the bands 1 and 2, with respect to the action $S_{\rm other}$, and σ^y is the usual Pauli matrix which acts on the space spanned by the two bands $\alpha = 1, 2$. (Notice that $G^{A/R/K}$ are 2×2 matrices because of the two bands.) The Pauli matrix σ^y and the negative frequencies $-\omega$ in some of the Green's functions come about because some of the propagators shown in Fig. (9) originate from the same vertex (or, equivalently, there are particle and hole propagators). We now observe that this series can be resumed and the trace can be greatly simplified:

$$\begin{aligned}
\partial_\delta \widetilde{\mathcal{L}}\left[\Delta, \delta\right]\big|_{\delta=0} = \frac{|\Delta|}{4\pi} \int (\mathrm{d}\boldsymbol{k}) \int \mathrm{d}\omega\ \mathrm{Tr} \Bigg[& \left(1 - \frac{|\Delta|^2}{4} G^R\left(\boldsymbol{k},\omega\right) \mathrm{i}\sigma_y G^A\left(\boldsymbol{k},-\omega\right) \mathrm{i}\sigma_y \right)^{-1} \\
& \times \left(G^R\left(\boldsymbol{k},\omega\right) \mathrm{i}\sigma_y G^K\left(\boldsymbol{k},-\omega\right) \mathrm{i}\sigma_y + G^K\left(\boldsymbol{k},\omega\right) \mathrm{i}\sigma_y G^R\left(\boldsymbol{k},-\omega\right) \mathrm{i}\sigma_y \right) \\
& \times \left(1 + \left(1 - \frac{|\Delta|^2}{4} G^A\left(\boldsymbol{k},\omega\right) \mathrm{i}\sigma_y G^R\left(\boldsymbol{k},-\omega\right) \mathrm{i}\sigma_y \right)^{-1} \frac{|\Delta|^2}{4} G^A\left(\boldsymbol{k},\omega\right) \mathrm{i}\sigma_y G^R\left(\boldsymbol{k},-\omega\right) \mathrm{i}\sigma_y \right) \Bigg] \\
+ \frac{|\Delta|}{4\pi} \int (\mathrm{d}\boldsymbol{k}) \int \mathrm{d}\omega\ \mathrm{Tr} \Bigg[& \left(1 - \frac{|\Delta|^2}{4} \mathrm{i}\sigma_y G^A\left(\boldsymbol{k},-\omega\right) \mathrm{i}\sigma_y G^R\left(\boldsymbol{k},\omega\right) \right)^{-1} \\
& \times \left(\mathrm{i}\sigma_y G^K\left(\boldsymbol{k},-\omega\right) \mathrm{i}\sigma_y G^A\left(\boldsymbol{k},\omega\right) + \mathrm{i}\sigma_y G^A\left(\boldsymbol{k},-\omega\right) \mathrm{i}\sigma_y G^K\left(\boldsymbol{k},\omega\right) \right) \\
& \times \left(1 + \left(1 - \frac{|\Delta|^2}{4} \mathrm{i}\sigma_y G^R\left(\boldsymbol{k},-\omega\right) \mathrm{i}\sigma_y G^A\left(\boldsymbol{k},\omega\right) \right)^{-1} \frac{|\Delta|^2}{4} \mathrm{i}\sigma_y G^R\left(\boldsymbol{k},-\omega\right) \mathrm{i}\sigma_y G^A\left(\boldsymbol{k},\omega\right) \right) \Bigg] .
\end{aligned} \tag{53}$$

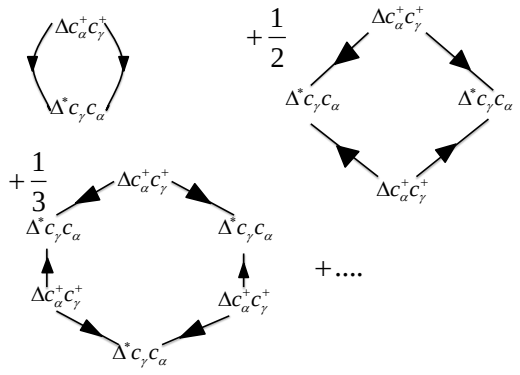

FIG. 9: Feynman diagrams. Series of ring diagrams that contribute to the action $\widetilde{S}[\Delta]$. Each line corresponds to a propagator $G^{A/R/K}$. The terms $1/n$ are symmetry factors for the diagrams.

In case the superconducting field $|\Delta|$ is small, this expression Eq. (53) may be further simplified:

$$\begin{aligned}
\approx & \frac{|\Delta|}{2}\int(\mathrm{d}\boldsymbol{k})\int\frac{\mathrm{d}\omega}{2\pi}\,\mathrm{Tr}\,\big[\mathrm{i}\sigma_y G^K(\boldsymbol{k},-\omega)\,\mathrm{i}\sigma_y G^A(\boldsymbol{k},\omega)+\mathrm{i}\sigma_y G^A(\boldsymbol{k},-\omega)\,\mathrm{i}\sigma_y G^K(\boldsymbol{k},\omega)\\
& \qquad +G^R(\boldsymbol{k},\omega)\,\mathrm{i}\sigma_y G^K(\boldsymbol{k},-\omega)\,\mathrm{i}\sigma_y+G^K(\boldsymbol{k},\omega)\,\mathrm{i}\sigma_y G^R(\boldsymbol{k},-\omega)\,\mathrm{i}\sigma_y\big]\\
& +\frac{|\Delta|^3}{8}\int(\mathrm{d}\boldsymbol{k})\int\frac{\mathrm{d}\omega}{2\pi}\,\mathrm{Tr}\,\big[\big(\mathrm{i}\sigma_y G^K(\boldsymbol{k},-\omega)\,\mathrm{i}\sigma_y G^A(\boldsymbol{k},\omega)+\mathrm{i}\sigma_y G^A(\boldsymbol{k},-\omega)\,\mathrm{i}\sigma_y G^K(\boldsymbol{k},\omega)\big)\\
& \qquad \times\big(\mathrm{i}\sigma_y G^A(\boldsymbol{k},-\omega)\,\mathrm{i}\sigma_y G^R(\boldsymbol{k},\omega)+\mathrm{i}\sigma_y G^R(\boldsymbol{k},-\omega)\,\mathrm{i}\sigma_y G^A(\boldsymbol{k},\omega)\big)\big]\\
& +\frac{|\Delta|^3}{8}\int(\mathrm{d}\boldsymbol{k})\int\frac{\mathrm{d}\omega}{2\pi}\,\mathrm{Tr}\,\big[\big(G^R(\boldsymbol{k},\omega)\,\mathrm{i}\sigma_y G^K(\boldsymbol{k},-\omega)\,\mathrm{i}\sigma_y+G^K(\boldsymbol{k},\omega)\,\mathrm{i}\sigma_y G^R(\boldsymbol{k},-\omega)\,\mathrm{i}\sigma_y\big)\\
& \qquad \times\big(G^R(\boldsymbol{k},\omega)\,\mathrm{i}\sigma_y G^A(\boldsymbol{k},-\omega)\,\mathrm{i}\sigma_y+G^A(\boldsymbol{k},\omega)\,\mathrm{i}\sigma_y G^R(\boldsymbol{k},-\omega)\,\mathrm{i}\sigma_y\big)\big]\ . \qquad (54)
\end{aligned}$$

Using the quantum regression theorem[28], one can compute the various Green's functions $G^R(\boldsymbol{k},\omega)=(\omega-H(\boldsymbol{k})+\mathrm{i}\hat{\Gamma})^{-1}$, $G^A(\boldsymbol{k},\omega)=(\omega-H(\boldsymbol{k})-\mathrm{i}\hat{\Gamma})^{-1}$ and $G^K(\boldsymbol{k},\omega)=G^R(\boldsymbol{k},\omega)\,(1-2f(\boldsymbol{k}))-(1-2f(\boldsymbol{k}))G^A(\boldsymbol{k},\omega)$. Here $H(\boldsymbol{k})\equiv\begin{pmatrix}\widetilde{E}_1(\boldsymbol{k}) & \Omega/2\\ \Omega/2 & \widetilde{E}_2(\boldsymbol{k})\end{pmatrix}$, $\hat{\Gamma}\equiv\begin{pmatrix}\Gamma_1 & 0\\ 0 & \Gamma_2\end{pmatrix}$ and $f(\boldsymbol{k})\equiv\begin{pmatrix}n_{\boldsymbol{k}}^{11} & n_{\boldsymbol{k}}^{21}\\ n_{\boldsymbol{k}}^{12} & n_{\boldsymbol{k}}^{22}\end{pmatrix}$. We may now perform the various traces and integrals over ω in Eq. (54) above. With this, we solve for the stationary conditions on the field Δ, coming from Eq. (51), and obtain

$$0=\frac{|\Delta|}{V}+|\Delta|\int(\mathrm{d}\boldsymbol{k})\,\mathrm{Re}\left\{\frac{1}{E_{\boldsymbol{k}}+\mathrm{i}\Gamma}\right\}\,(1-n_{\boldsymbol{k}}^{11}-n_{\boldsymbol{k}}^{22})-4\,|\Delta|^3\int(\mathrm{d}\boldsymbol{k})\,\mathrm{Re}\left\{\frac{1}{E_{\boldsymbol{k}}+\mathrm{i}\Gamma}\right\}\,\frac{1-n_{\boldsymbol{k}}^{11}-n_{\boldsymbol{k}}^{22}}{E_{\boldsymbol{k}}^2+\Gamma^2}\ . \qquad (55)$$

The part involving $\mathrm{Re}\left\{\frac{1}{E_{\boldsymbol{k}}+\mathrm{i}\Gamma}\right\}$ is exact and comes about because the Keldysh action must be real. In the third term of Eq. (55), we have also made the assumption that $\Omega\gg\Gamma$. Using the non-equilibrium population deviation $1-n_{\boldsymbol{k}}^{11}-n_{\boldsymbol{k}}^{22}$ given in Eq. (13) for small $|\Delta|$ we see that this agrees to leading order for small $|\Delta|$ with Eq. (19); a computation of the exact trace in Eq. (53) would presumably reproduce Eq. (19) to all orders.

V. CONCLUSIONS

We have demonstrated that superconductivity can be achieved in a laser-driven two-band semiconductor interacting with reservoir – either in the form of a tunneling contact to a metal, or in the form of other modes in the band, or in the form of a third band (see appendix). The superconductivity is robust to changes in temperature, and under optimal conditions, the size of the superconducting gap scales with the decay rate Γ. We found that depending on the sign of the band curvatures, it is possible to obtain superconducting pairing $s_{\boldsymbol{k}}^{21}$ with both repulsive and attractive interactions. We can estimate how stringent is the condition given in Eq. (22) for the threshold for producing

superconductivity with two bands and reservoirs. To do so we compare our results to regular BCS theory. At zero temperature, the BCS gap equation may be written as $V\rho\left(k_{\mathrm{F}}\right)\ln\left(\frac{\omega_{\mathrm{D}}}{\Delta}\right)=1$. Here $\rho\left(k_{\mathrm{F}}\right)$ is the density of states at Fermi energy and ω_{D} is the Debye frequency. Using the experimentally relevant parameters $\omega_{\mathrm{D}}\sim 100K$ and $\Delta\sim 1K$ we obtain $V\rho\left(k_{\mathrm{F}}\right)\sim 0.2$. We note that V is the effective electron-electron interaction which includes the effects of phonons and screening. For the superconductivity proposed in this manuscript we have obtained the threshold equation $\frac{|V|\,N_0|v_-|}{|\kappa|^{1/2}\Gamma^{1/2}}>1$. Using $\kappa\sim\left(10^6 eV\right)^{-1}c^2$, $\Gamma\sim 10^{-3}eV$, $|v_-|\sim 10^{-2}c$ this condition simplifies to $0.2\times 10^{2.5}>1$ which is easily satisfied. We note that for the case of repulsive interactions $|V|\,N_0$ can be larger. These numbers are relevant for room temperature superconductivity. We note that the same threshold condition shows up in the case of an optically pumped two-band semiconductor considered in Sect. III and in the case where the laser Rabi frequency is small but the two decay rates are very different, see Eqs. (32) and (44). Eq. (46) establishes that all our results are unaffected by mismatches in the Fermi velocities of the upper and lower band as long as these mismatches are only roughly ten percent of the Fermi velocity. The present results are also insensitive to imprecision in tuning the right μ on the order of 0.01 eV. We note that imperfections in finding the right μ do not effect the results presented in Sect. III as the condition $E_1\left(\boldsymbol{k}\right)+E_2\left(-\boldsymbol{k}\right)=0$ is automatically selected. Even though T_{c} (critical temperature for superconductivity) does not scale with the gap for our setup, as in the case of a regular superconductor, we note that under optimal conditions it is possible to achieve a gap that is several hundred Kelvins.

We unveiled a new route to induce superconductivity, not simply by lowering the temperature of the sample but by shining light. In a semiconductor, such photo-induced superconductivity is possible at temperatures smaller than the band gap, which itself is a very high temperature. Hence, the mechanism may enable dissipationless current transport for frequencies smaller than that set by the superconducting gap at room temperature. In many ways the ultimate limit on our setup is the temperature dependence of the rate Γ. T_c is set by the relationship $\frac{|V|\,N_0|v_-|}{|\kappa|^{1/2}\Gamma^{1/2}(T_c)}=1$. Additionally, one can imagine applications where the superconductivity is induced for short periods of time by laser pulses and is allowed to decay when the laser is turned off. This opens the door for superconducting switches. We intend to perform a DMFT analysis of the phenomena to study the effects of strong correlations and strong laser driving. We shall also study the optical response of the proposed superconductor as well as investigate the possibility of a Josephson effect.

Acknowledgments

This work has been supported by the Rutgers CMT fellowship (G.G.), the NSF grants DMR-0906943 and DMR-115181 (C.A.), and the DOE Grant DEF-06ER46316 (C.C.). We would like to thank L. Levitov, G. Kotliar and D. Khmelnitskii for pointing out useful references.

Appendix A: Three-band semi-conductor

Let us consider superconductivity in an optically pumped three-band semiconductor. The lower (1), middle (3) and upper (2) bands have dispersion relations $E_\alpha(\boldsymbol{k})$ with $\alpha=1$, 2, 3. The third band can be seen as a replacement for the reservoirs that were required in the case considered in Sect. II. We assume that the dispersion is symmetric so that $E_\alpha\left(\boldsymbol{k}\right)=E_\alpha\left(-\boldsymbol{k}\right)$, for $\alpha=1$, 2 – this will allow for s-wave superconductivity without any energy mismatch. The upper and lower bands are resonantly driven by a single laser with frequency ω_0, *i.e.* $E_2\left(\boldsymbol{k}_0\right)=E_1\left(\boldsymbol{k}_0\right)+\omega_0$ for some wave vectors $\boldsymbol{k}_0$. In our scheme, the middle band 3 (reservoir) is not coupled to any laser but will simply ensure that there is less then one electron per $\boldsymbol{k}$ value in the upper and lower bands combined, $n_{\boldsymbol{k}}^{11}+n_{\boldsymbol{k}}^{22}<1$. This inequality satisfies the condition that the population of the two bands involved in the pairing deviates from unity, which was the requisite for superconductivity in Sect. II. We set the chemical potential μ in between the lower and middle band, *i.e.* $E_2>E_3>\mu>E_1$ for all wave vectors $\boldsymbol{k}$, see Fig. (10). More precisely, we set $\mu=[E_2(\boldsymbol{k}_0+E_1(\boldsymbol{k}_0)]/2$; this ensures that all quasiparticles have zero energy. In the rotating frame, this will correspond to a zero energy condition for the electrons at $\boldsymbol{k}_0$.

To favor superconductivity, we assume that the level sets of $E_1\left(\boldsymbol{k}_0\right)$ and $E_2\left(\boldsymbol{k}_0\right)$ have a good overlap and that the electron velocities of the lower and upper bands are opposite at the wave vector $\boldsymbol{k}_0$. Under such conditions, we find that depending on the curvature of the lower and upper bands at $\boldsymbol{k}_0$ it is possible to induce superconductivity with *either repulsive or attractive interactions*, in particular to obtain a non-vanishing anomalous correlator $\left\langle c_{\boldsymbol{k}}^2 c_{-\boldsymbol{k}}^1\right\rangle\equiv s_{\boldsymbol{k}}^{21}$. The analysis presented in this Appendix is highly similar to the one done in the body of the manuscript and will be presented briefly.

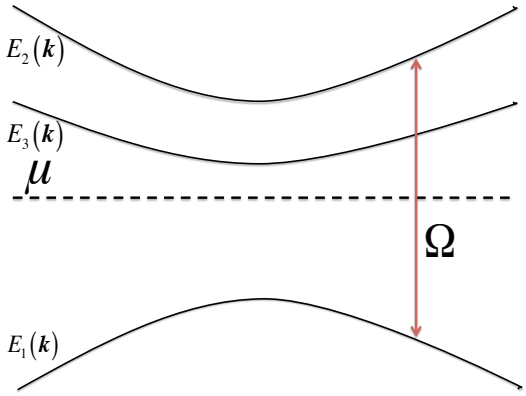

FIG. 10: Energy levels and laser. The upper band of a three-band semiconductor is populated with a single laser drive pumping from the lower band. The chemical potential μ is set between the lower and middle (reservoir) bands.

1. Mean-field Hamiltonian

The mean-field Hamiltonian relevant to our three-band system can be written as:

$$H_{\mathrm{MF}} = H_{\mathrm{Band}} + H_{\mathrm{Laser}} + H_{\mathrm{Super}} \,, \tag{A1}$$

with

$$H_{\mathrm{Band}} = \sum_{\boldsymbol{k},\alpha} E_\alpha\left(\boldsymbol{k}\right) c_{\boldsymbol{k}}^{\alpha\dagger} c_{\boldsymbol{k}}^{\alpha} \,, \tag{A2}$$

$$H_{\mathrm{Laser}} = \sum_{\boldsymbol{k}} \Omega\left(t\right) c_{\boldsymbol{k}}^{2\dagger} c_{\boldsymbol{k}}^{1} + \ \mathrm{h.c.} \,, \tag{A3}$$

$$H_{\mathrm{Super}} = \sum_{\boldsymbol{k}} \Delta c_{\boldsymbol{k}}^{2\dagger} c_{-\boldsymbol{k}}^{1\dagger} + \ \mathrm{h.c.} \,. \tag{A4}$$

$\Omega\left(t\right) \equiv \Omega \cos\left(\omega_0 t\right)$ is the laser drive and Δ is the mean-field superconducting gap. The relevant equation of motions read

$$\begin{aligned}
\mathrm{i}\frac{\mathrm{d}}{\mathrm{d}t} c_{\boldsymbol{k}}^{2} =& \Delta c_{-\boldsymbol{k}}^{1\dagger} + E_2 c_{\boldsymbol{k}}^{2} + \Omega\left(t\right) c_{\boldsymbol{k}}^{1} \,, \\
\mathrm{i}\frac{\mathrm{d}}{\mathrm{d}t} c_{\boldsymbol{k}}^{3} =& E_3 c_{\boldsymbol{k}}^{3} \,, \\
\mathrm{i}\frac{\mathrm{d}}{\mathrm{d}t} c_{\boldsymbol{k}}^{1} =& -\Delta c_{-\boldsymbol{k}}^{2\dagger} + E_1 c_{\boldsymbol{k}}^{1} + \Omega^*\left(t\right) c_{\boldsymbol{k}}^{2} \,.
\end{aligned} \tag{A5}$$

We eliminate all explicit time dependence by a means of rotating wave approximation. This consists in rotating all the operators of the theory with the unitary

$$U \equiv U_c \otimes U_a \,, \tag{A6}$$

where

$$U_c \equiv \exp\left[\frac{\mathrm{i}}{2}\omega_0 t \sum_{\boldsymbol{k}} \left(c_{\boldsymbol{k}}^{1\dagger} c_{\boldsymbol{k}}^{1} - c_{\boldsymbol{k}}^{2\dagger} c_{\boldsymbol{k}}^{2}\right)\right] \,, \tag{A7}$$

$$U_a \equiv \exp\left[\frac{\mathrm{i}}{2}\omega_0 t \sum_{\boldsymbol{k},n} \left(a_{\boldsymbol{k},n}^{1\dagger} a_{\boldsymbol{k},n}^{1} - a_{\boldsymbol{k},n}^{2\dagger} a_{\boldsymbol{k},n}^{2}\right)\right] \,. \tag{A8}$$

In particular, $c_{\boldsymbol{k}}^{1} \mapsto \widetilde{c}_{\boldsymbol{k}}^{1} = c_{\boldsymbol{k}}^{1}\,\mathrm{e}^{-\mathrm{i}\omega_0 t/2}$, $c_{\boldsymbol{k}}^{2} \mapsto \widetilde{c}_{\boldsymbol{k}}^{2} = c_{\boldsymbol{k}}^{2}\,\mathrm{e}^{\mathrm{i}\omega_0 t/2}$, and $H \mapsto \widetilde{H} = U\left[H - \mathrm{i}\partial_t\right]U^\dagger$ so that the energies are shifted to $\widetilde{E}_1(\boldsymbol{k}) = E_1(\boldsymbol{k}) + \omega_0/2$ and $\widetilde{E}_2(\boldsymbol{k}) = E_2(\boldsymbol{k}) - \omega_0/2$. We drop all terms rotating at $2\omega_0$ since they are not

resonant with any transition. By adding dissipative mechanisms and considering fermion bilinears we may study the non-equilibrium steady state properties of this model. Note that in the rotating frame, $\widetilde{n}^{11}_{\boldsymbol{k}} = n^{11}_{\boldsymbol{k}}$, $\widetilde{n}^{22}_{\boldsymbol{k}} = n^{22}_{\boldsymbol{k}}$, and $\widetilde{s}^{12}_{\boldsymbol{k}} = s^{12}_{\boldsymbol{k}}$ are invariant, but $\widetilde{n}^{12}_{\boldsymbol{k}} = n^{12}_{\boldsymbol{k}}\,\mathrm{e}^{-\mathrm{i}\omega_0 t}$ and $\widetilde{n}^{21}_{\boldsymbol{k}} = n^{21}_{\boldsymbol{k}}\,\mathrm{e}^{\mathrm{i}\omega_0 t}$. The steady-state equation of the order-parameter $\widetilde{s}^{21}_{\boldsymbol{k}} = \langle \widetilde{c}^{2}_{\boldsymbol{k}} \widetilde{c}^{1}_{-\boldsymbol{k}} \rangle$ reads

$$0 = \mathrm{i}\frac{\mathrm{d}}{\mathrm{d}t}\widetilde{s}^{\dagger 21}_{\boldsymbol{k}} = -\Delta^*(1 - \widetilde{n}^{11}_{\boldsymbol{k}} - \widetilde{n}^{22}_{\boldsymbol{k}}) - (\widetilde{E}_{\boldsymbol{k}} - \mathrm{i}\Gamma_{12})\widetilde{s}^{\dagger 21}_{\boldsymbol{k}} \,, \tag{A9}$$

where we introduced the notation $\widetilde{E}_{\boldsymbol{k}} \equiv \widetilde{E}_1(\boldsymbol{k}) + \widetilde{E}_2(\boldsymbol{k})$ and Γ_{12} is a phenomenological decay rate associated with the damping of the order parameter. This simplifies to

$$\widetilde{s}^{21}_{\boldsymbol{k}} = \frac{\Delta^*}{\widetilde{E}_{\boldsymbol{k}} + \mathrm{i}\Gamma_{12}} \left(\widetilde{n}^{11}_{\boldsymbol{k}} + \widetilde{n}^{22}_{\boldsymbol{k}} - 1 \right) \,. \tag{A10}$$

This equation is identical to Eq. (10) and seems to be an ubiquitous condition for superconductivity. This expresses that to ensure superconductivity, we once again need to have a nonzero $\widetilde{n}^{11}_{\boldsymbol{k}} + \widetilde{n}^{22}_{\boldsymbol{k}} - 1 \neq 0$. This is the rationale behind the presence of the third band – which does not interact with the other two bands but merely acts as "storage" for electrons. To find the steady-state value of $\widetilde{n}^{11}_{\boldsymbol{k}}$ and $\widetilde{n}^{22}_{\boldsymbol{k}}$, we write the steady-state equations for the rest of the fermion bilinears. From now on, we shall work in the weak pairing field limit $\Delta \ll \Omega$. The steady-state equations for the populations and coherences read

$$\begin{aligned}
0 = \frac{\mathrm{d}}{\mathrm{d}t}\widetilde{n}^{22}_{\boldsymbol{k}} =& \mathrm{i}\frac{\Omega}{2}\left(\widetilde{n}^{12}_{\boldsymbol{k}} - \widetilde{n}^{21}_{\boldsymbol{k}}\right) - (\Gamma_1 + \Gamma_2)\,\widetilde{n}^{22}_{\boldsymbol{k}} \,, \\
0 = \frac{\mathrm{d}}{\mathrm{d}t}\widetilde{n}^{33}_{\boldsymbol{k}} =& \Gamma_1 n^{22}_{\boldsymbol{k}} - \Gamma_3 n^{33}_{\boldsymbol{k}} \,, \\
0 = \frac{\mathrm{d}}{\mathrm{d}t}\widetilde{n}^{11}_{\boldsymbol{k}} =& -\mathrm{i}\frac{\Omega}{2}\left(\widetilde{n}^{12}_{\boldsymbol{k}} - n^{21}_{\boldsymbol{k}}\right) + \Gamma_2\widetilde{n}^{22}_{\boldsymbol{k}} + \Gamma_3\widetilde{n}^{33}_{\boldsymbol{k}} \,, \\
0 = \frac{\mathrm{d}}{\mathrm{d}t}\widetilde{n}^{21}_{\boldsymbol{k}} =& (\mathrm{i}\varepsilon_{\boldsymbol{k}} - \tau^{-1})\widetilde{n}^{21}_{\boldsymbol{k}} + \mathrm{i}\frac{\Omega}{2}\left(\widetilde{n}^{11}_{\boldsymbol{k}} - \widetilde{n}^{22}_{\boldsymbol{k}}\right) \,.
\end{aligned} \tag{A11}$$

We have introduced three spontaneous decay rates $\Gamma_1, \Gamma_2, \Gamma_3$ and a dephasing time τ. For many semiconductors $\tau^{-1} \gg \Gamma_{1,2,3}$ because it is hard to exchange populations between the bands, by including say Coulomb interactions, but rather easy to have energy fluctuations which lead to dephasing. In the case the semiconductor has a strong coupling to optical phonons, this inequality may be violated as all the decay rates may become comparable. Notice that the previous equations ensure the conservation of particle number, *i.e.* $\widetilde{n}^{11}_{\boldsymbol{k}} + \widetilde{n}^{22}_{\boldsymbol{k}} + \widetilde{n}^{33}_{\boldsymbol{k}} = 1$. Using Eq. (A10), we obtain

$$s^{\dagger 21}_{\boldsymbol{k}} = -\frac{\Delta^*}{\widetilde{E}_{\boldsymbol{k}} + \mathrm{i}\Gamma_{12}} \frac{\frac{|\Omega|^2\Gamma_1}{2\tau\left(\varepsilon^2_{\boldsymbol{k}} + \tau^{-2}\right)}}{\Gamma_3\left(\Gamma_1 + \Gamma_2\right) + \frac{|\Omega|^2(\Gamma_1 + 2\Gamma_3)}{2\tau\left(\varepsilon^2_{\boldsymbol{k}} + \tau^{-2}\right)}} \,, \tag{A12}$$

with $\varepsilon_{\boldsymbol{k}} \equiv \widetilde{E}_2(\boldsymbol{k}) - \widetilde{E}_1(\boldsymbol{k})$.

Note that $s^{\dagger 21}_{\boldsymbol{k}}$ vanishes when $\Gamma_1 = 0$ but $\Gamma_3 \neq 0$. In this case there is no population in the the middle band, *i.e.* $\widetilde{n}^{33}_{\boldsymbol{k}} = 0$. However, one would not expect that $s^{\dagger 21}_{\boldsymbol{k}} = 0$ if we simultaneously tune $\Gamma_1, \Gamma_3 \downarrow 0$ as some population will be trapped in band 3 (reservoir) if both decay rates go down to zero with the same rate, which can be seen from the analysis of Eq. (A12).

2. Self-Consistency Equation

We now solve self-consistently for the superconducting gap. The pairing part of the mean-field Hamiltonian in Eq. (A1) originates from a microscopic Hamiltonian which involves a density-density type of interaction between the electrons in the semiconductor. The corresponding mean-field decoupling is given in Eq. (39). To obtain most favorable conditions for superconductivity, we shall once again assume that the electron velocities of the lower and upper bands are opposite at the wave vector $\boldsymbol{k}_0$. At the resonant surface $\mathcal{S}_{\omega_0}$, the dispersion relation can be Taylor-expanded as $\widetilde{E}_{1,2} = v_{1,2}\,q_\perp + \kappa_{1,2}\,q_\perp^2 + \ldots$, where $q_\perp$ is the momentum perpendicular to the resonant surface $\mathcal{S}_{\omega_0}$ and $v_1 + v_2 = 0$. So $\varepsilon = v_-\,q_\perp + \kappa_-\,q_\perp^2 + \ldots$ and $E = \kappa_+\,q_\perp^2 + \ldots$, where $v_- \equiv v_2 - v_1$ and $\kappa_\pm = \kappa_2 \pm \kappa_1$. Substituting these energies into the gap equation, we obtain the condition

$$\Delta^* \leq -VN_0\left|v_-\right| \int \mathrm{d}q_\perp \frac{\Delta^*\kappa_+ q_\perp^2}{\kappa_+^2 q_\perp^4+\Gamma_{12}^2} \; \frac{\frac{|\Omega|^2\Gamma_1}{2\tau\left(\left(v_- q_\perp\right)^2+\tau^{-2}\right)}}{\Gamma_3(\Gamma_1+\Gamma_2)+\frac{|\Omega|^2(\Gamma_1+2\Gamma_3)}{2\tau\left(\left(v_- q_\perp\right)^2+\tau^{-2}\right)}} \; . \tag{A13}$$

N_0 is the density of states at $\boldsymbol{k}_0$. We note that

$$\operatorname{sgn} V = \operatorname{sgn} \kappa_+ \tag{A14}$$

is needed to satisfy the condition, which means that by tuning band curvatures it is possible to have superconductivity with *both attractive and repulsive interactions*. Furthermore, we note that in the case in which the Rabi frequency is large, the integral in Eq. (A13) greatly simplifies and the threshold condition for superconductivity becomes

$$|V| \geq V_\mathrm{c} \equiv \frac{\sqrt{2}}{\pi}\frac{1}{N_0}\frac{\sqrt{|\kappa_+|}}{|v_-|}\sqrt{\Gamma_{12}}\left(1+2\Gamma_3/\Gamma_1\right) \; . \tag{A15}$$

In the small damping limit (*i.e.* small Γ_{12}), the inequality is easily satisfied. This condition is highly similar to the condition obtained for superconducting threshold in Eq. (22). We note that for the case $\gamma_2-\gamma_1 \sim 1$, $\Gamma_{12} \sim \Gamma$, and $\Gamma_1 \gg \Gamma_3$ the two equations become equivalent.

[1] M. Tinkham, *Introduction to superconductivity* (Dover Publications, 1996).
[2] P. W. Anderson, *The theory of superconductivity in the high T_c cuprates*, (Princeton university press 1997).
[3] D. C. Johnston, Advances in Physics **59**, 803 (2010).
[4] Q. Si and E. Abrahams, Phys. Rev. Lett. **101**, 076401 (2008).
[5] J. E. Mooij, T. P. Orlando, L. Levitov, L. Tian, C. H. van der Wal and S. Lloyd, Science **285**, 1036 (1999).
[6] J. Q. You, J. S. Tsai and F. Nori, Phys. Rev. Lett. **89**, 197902 (2002).
[7] M. N. Wilson, *Superconducting magnets* (Clarendon press 1983).
[8] A. Mourachkine, *Room temperature superconductivity* (Cambridge International Science publishing 2004).
[9] D. H. Dunlap, and V. M. Kenkre, Phys. Rev. B **34**, 3625 (1986).
[10] M. Holthaus, Phys. Rev. Lett. **69**, 351 (1992).
[11] H. Lignier, C. Sias, D. Ciampini, Y. Singh, A. Zenesini, O. Morsch, and E. Arimondo, Phys. Rev. Lett. **99**, 220403 (2007).
[12] C. E. Creffield and T. S. Monteiro, Phys. Rev. Lett. **96**, 210403 (2006).
[13] A. Eckardt, C. Weiss, and M. Holthaus, Phys. Rev. Lett. **95**, 260404 (2005).
[14] A. Zenesini, H. Lignier, D. Ciampini, O. Morsch, and E. Arimondo, Phys. Rev. Lett. **102**, 100403 (2009).
[15] J. Struck, C. Ölschläger, R. Le Targat, P. Soltan-Panahi, A. Eckardt, M. Lewenstein, P. Windpassinger, and K. Sengstock, Science **333**, 996 (2011).
[16] N. Tsuji, T. Oka, P.Werner, and H. Aoki, Phys. Rev. Lett. **106**, 236401 (2011).
[17] N. Tsuji, T. Oka, H. Aoki, and P. Werner, Phys. Rev. B **85**, 155124 (2012).
[18] N. Tsuji, T. Oka, and H. Aoki, Phys. Rev. B **78**, 235124 (2008).
[19] V. F. Elesin, Sov. Phys. JETP 32, 328 (1971).
[20] V. M. Galitskii, V. F. Elesin and Yu. V. Kopaev, ZhETF Pis. Red. 18, 50 (1973).
[21] D. A. Kirshnits and Yu. V. Kopaev, ZhETF Pis. Red. 17, 379 (1973).
[22] V. F. Elesin, Yu. V. Kopaev and R. Kh. Timerov, Zh. Eksp. Teor. Fiz. 2343 (1973).
[23] V. M. Galitskii, S. P. Goreslavskii and V. F. Elesin Zh. Eksp. Theor. Fiz. 57, 207 (1969).
[24] It is not strictly necessary that each wave vector k corresponds to its own reservoir. All that is needed is that $\langle t^*(k)\, t(k')\rangle \sim \delta(k-k')$ which would happen for a disordered metal reservoir.
[25] R. R. Puri, *Mathematical Methods of Quantum Optics,* (Springer Verlag 2001).
[26] H. Haug and S. W. Koch, *Quantum theory of the optical and electronic properties of semiconductors*, (World Scientific Publishing co. 1990).
[27] W. W. Chow, S. W. Koch and M. Sargent, *Semiconductor-laser physics* (Springer-Verlag 1994).
[28] H. G. Carmichael, *Statistical Methods in Quantum Optics 1: Master Equations and Fokker-Plank Equations*, (Springer Verlag 1999).